ALMA MATER STUDIORUM
UNIVERSITÀ DEGLI STUDI DI BOLOGNA

Seconda Facoltà di Ingegneria con sede a Cesena
Corso di Laurea Magistrale in Ingegneria Elettronica e
Telecomunicazioni per lo sviluppo sostenibile

ANALYSIS AND IMPLEMENTATION OF
TIME-OF-ARRIVAL ESTIMATION
TECHNIQUES OF UWB SIGNALS

Elaborato in: Reti di sensori wireless per monitoraggio
ambientale

Tesi di Laurea di:
RICCARDO FOIERA

Relatore:
Chiar.mo Prof. Ing. DAVIDE
DARDARI

Correlatori:
Dott. Ing. NICOLÓ DECARLI
Dott. Ing. FRANCESCO GUIDI

ANNO ACCADEMICO 2010–2011
SESSIONE III

Keywords

UWB

RTLS

RFID

Backscatter modulation

Time-of-Arrival

To those who have believed and still believe in me,

Contents

Introduction

More and more frequently nowadays we feel the need to locate everything and everywhere; starting from ourselves along the streets to get to the goods in stock.

The increased interest in real-time localization can be felt by looking the dividing of global revenues; in fact the amount of global revenues for real-time locating systems (RTLSs) will rise to six billions by 2017 [2]. Many different techniques in literature are proposed to achieve this goal, but the most rated one is the Time-of-Arrival (ToA) estimation, that using a simple mathematical relation, allows to know the distance between two objects. Starting from the time of flight of a signal, the distance is measured.

Thus a system that gives the possibility to measure, as accurately as possible, the ToA of a signal becomes a very stringent requirement to enhance the ranging accuracy. The use of back-scattering modulation with UWB signals in RFID scenarios seems to be the best solution for applications where, in addition to good Ranging performance, the low power consumption and low complexity for the tags is important.

But what does UWB and RFID mean? UWB is an acronym of Ultra WideBand; that is a wireless communication technique used to transmit and receive signals with very short time duration (i the order of a few ns) and with a very low transmitting power. This gives the possibility to introduce a telecommunication system that works in a scenario with others systems without creating interference to the already existent technology. But the short signals make also possible a high resolution in multipath environment. RFID instead means Radio Frequency IDentification; it is a technology for the identification and informations exchange between two actors, a *reader* and a *tag*. The reader makes an interrogation to the tag, and the tag answers with

the information required by the reader.

These technologies are those investigated in the European project SE-LECT to which thesis is inspired [1]. Thanks to this answer we can estimate the ToA and then locate the tag in our scenario.

SELECT project [1] aims to combine the technologies above mentioned. Like the title suggests, the main topic of this work is the analysis of ToA estimation techniques of UWB signals for RFID scenarios.

An overview of basic concepts in chapter 1 is reported, and a brief discussion on ranging with UWB signal in chapter 2 is conducted. In chapter 3, ToA estimations algorithm are described, with particular emphasis on techniques implemented in a Matlab simulator, and numerical results are reported. Finally a practical ToA estimator is shown in chapter 4, whose performance is analyzed. A brief summary and the comparison on the results in the conclusion are reported.

Chapter 1

UWB for RFID systems

1.1 UWB signal

FCC (Federal Communication Commission) defines an Ultra Wide-Band signal as a signal that occupies more than 500MHz of the frequency's spectrum or has got a fractional bandwidth BF (as defined in (1.1)) in excess of 20%.

$$BF = \frac{f_H - f_L}{\frac{(f_H + f_L)}{2}} \geq 0.2 \qquad (1.1)$$

Moreover it has to have a maximum EIRP equal to -41.25 dBm/MHz to be irradiated[2].
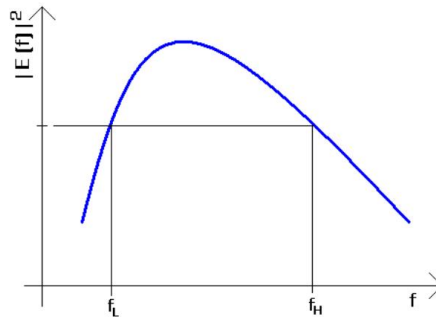
Figure 1.1: Example of spectrum for UWB signal [2].

The main advantages given by UWB signals have to be found in high temporal resolution, multiple access, low probability of detection and underlay technology.

This kind of signals can be realized by the adoption of Impulse Radio (IR) technique that ensures low complexity.

UWB signals are typically composed of a train of pulses, modulated by Pulse Position Modulation (PPM) or Pulse Amplitude Modulation (PAM). Deriving Gaussian pulse $p_0(t) = \exp(-2\pi(t^2/\tau_p^2))$ [2] we can obtain an example of pulse used, and in this way we can respect spectrum mask imposed by FCC or other administrative bodies.
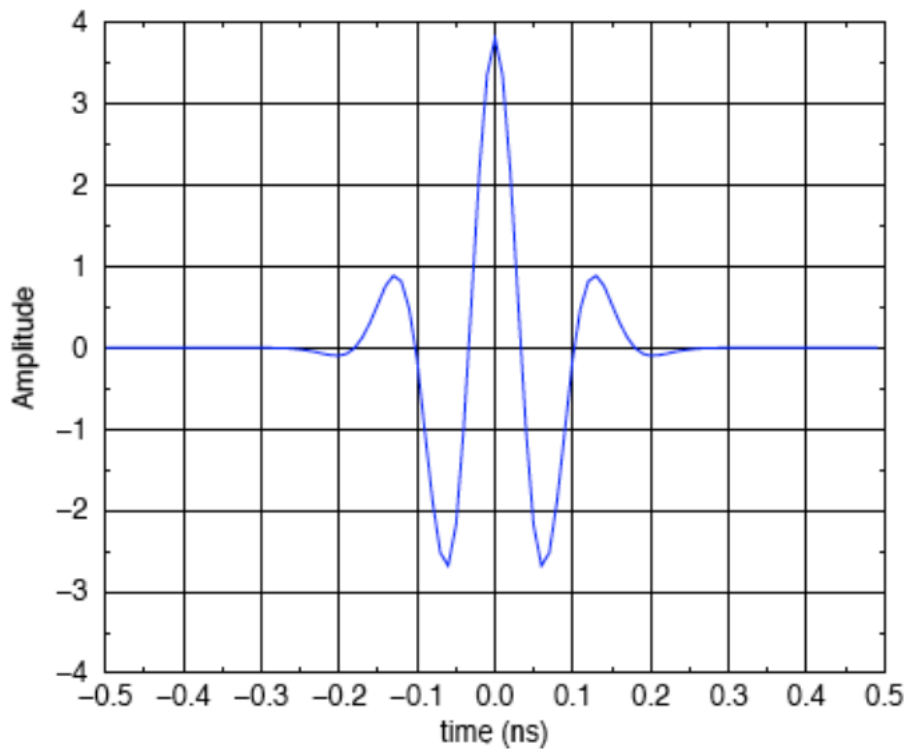
Figure 1.2: Example of Gaussian 6-th derivative monocycle [2].

1.2   RFID overview

RFID technology is used for real-time objects identification in many different fields; from logistic to automation systems etc. This technology is composed of two actors: reader and tag (see Fig. 1.3). The dialogue between reader and tag takes place when the reader makes an interrogation by transmitting a wireless signal to the tag. The answer of the tag is composed by a signal that returns to the reader modulated by the stored information.
We can distinguish between three different kinds of RFID systems:

- *Active RFID*, where tags are powered to ensure the answer (an active transmission of power) and the data collection and maintenance.

- *Semi-active* or *semi-passive RFID*, where tags are powered only for data maintenance. The power for the answer is taken by the interrogation signal. (i.e. backscatter modulation of the incident signal)

- *Passive RFID*, where tags are no powered. The only power used is given by the interrogation signal.

All this kind of RFIDs are used in many fields, but for some particular applications is important to reduce low power consumption, and the system complexity and dimensions; for all this reasons *semi-passive RFIDs* are adopted in SELECT project [1].
A RFID system usually is composed of many tags and one or more readers located in known positions. In addition to the data information received by the tags, it is possible to estimate the distance between tag and reader if UWB technology is adopted. This estimation can be done multiplying the speed of the signal for the time employed to travel the distance between reader and tag. In this way, at the same time, it is possible to collect data from tags and keep information about the distance between tag and reader. This technique has been chosen for SELECT applications because combined with UWB signals makes possible centimetre resolution for ranging applications.

1.3   Real-Time Locating Systems

Acronym RTLSs means real-time locating systems. This systems nowadays are important for a lot of applications (logistic, security tracking, medical services, rescue operations, military systems and so on) where real-time location plays the key role. The most popular RTLS used by many people all over the world is global positioning systems (GPS); this satellite-based system makes possible for people with ground receivers to determine their geographic location [2]. GPS is often used for transportation application; in particular intelligent transportation systems (ITSs) for traffic routing, roadside assistance and cargo tracking are used.

Other interesting applications for RTLSs are *high-definition situation-aware* (HDSA) systems, capable of working in harsh environments like caves or inside building where GPS fails and applications where high positioning accuracy is required [2].

RTLS bases its work on wireless transmission of a signal used to locate (and eventually to keep other information) people or object. In this field we can distinguish two kind of positioning [2]:

- *position location* which implies the presence of an "active" terminal whose position has to be determined;

- *radio-location* which usually refers to find a "passive" object that does not obligated to collaborate in radio localization.

Thus, there are many different families of systems referred to the same term "position location". Usually wireless positioning systems have a number of wireless nodes (*anchor* nodes) at a fixed and precise known location in a coordinate reference frame and one ore more mobile (*target*) nodes to be located [2]. Positioning is usually done in two steps: at first the measurements are performed, and second these measurements are processed to perform the position of target nodes.

A classification for RTLSs can be done looking at the method implemented for the distance estimation. Considering the radio signal characteristics we can list:

- the received signal strength (RSS),

- time of arrival (ToA),

- angle of arrival (AoA),

- near field ranging (NFR),

- the knowledge of two or more nodes in radio visibility.

In addition *inertial* (like angular velocity and acceleration) and *Earth magnetic field* informations may be also considered for positioning location systems [2]. Other kind of classification for RTLSs can be done, for example satellite-based or terrestrial-based systems. RFID technologies can classified in RTLSs terrestrial network-based systems, and will be used for SELECT project [1].

1.4   UWB backscatter modulation

Backscattering modulation is a technique used in RFID systems where the tag is interrogated by the reader to receive its stored information. This modulation consists of changing antenna reflection properties (the load) according to information data. In fact, when an electromagnetic wave encounters an antenna, it is partially reflected back depending on the antenna configuration [3].
According to this mechanism we can have two kinds of backscattering: *structural mode* and *antenna mode*.

- *Structural mode* depends by the shape and the material of the antenna, and does not change with different antenna loads.

- *Antenna mode* instead depends by the load applied to the tag, and thus, the data can be sent back without a dedicated power source, but only with a proper load variation.

As shown in Fig. 1.3 we can see the two scattering mode resulting from the reflection of the transmitted pulse. The antenna mode scattered signal can be varied according to the antenna load Z_L, whereas structural mode does not change. In this way we can distinguish three different cases:

- $Z_L = \infty$ open circuit ($\varphi_{incident} - \varphi_{scattered} = 0$),

- $Z_L = Z_A^*$ matched load (no reflected wave),

- $Z_L = 0$ short circuit $(\varphi_{incident} - \varphi_{scattered} = \pi)$,

where Z_A is the antenna impedance [3] and φ is the phase of the incident or scattered signal.

Usually, in a realistic scenario the sum of the structural mode scattering (that is one or two order of magnitude greater than antenna mode scattering) and the presence of objects in the surrounding scenario (clutter component of the signal scattering) cause a degradation of the useful signal at the reader side [3].
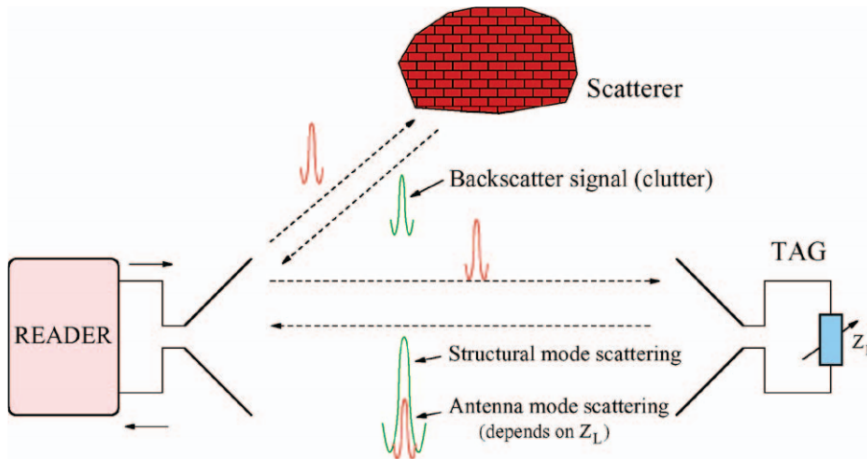
Figure 1.3: Examples of backscattering mechanism [2].

Chapter 2

Ranging with UWB signals

2.1 Time-Based Ranging

Ranging with UWB signals is possible thanks to *Time-of-Arrival* (ToA) estimation. If the propagation velocity (v) of the signal is known, measuring the *time of flight* τ_f, we can calculate the distance between two objects (in our case tag and reader) by:

$$d = \tau_f \cdot v \tag{2.1}$$

In our case, v is the speed of light($\simeq 3 \cdot 10^8$ [m/s]).
This simple technique is the base for some of the most used ToA techniques described below.

One-Way ToA Ranging[4][2] At time t_1 node A transmits a packet, which contains timestamp t_1, to node B. B receives the packet at time t_2 and under ideal conditions (clock A and B are perfectly synchronized with a reference clock) $\tau_f = t_2 - t_1$. Now we can calculate the distance between A and B using (2.1).
But if the nodes are not synchronized significantly errors can affect ranging estimation; so a good synchronization technique is required for One-Way ToA ranging.

Two-Way ToA Ranging[4][2] Two-Way ToA ranging aims to solve the problem of a non common time reference. In this technique,

Figure 2.1: Example of One-Way ToA Ranging [2].

node A transmits a packet to node B, and after τ_d seconds, B retransmits the packet to A. The estimated round-trip-time (RTT) at A is $\tau_{RT} = 2\tau_f + \tau_d$. If τ_d is known, we can estimate the distance again using (2.1). Despite with this method the synchronization effects are
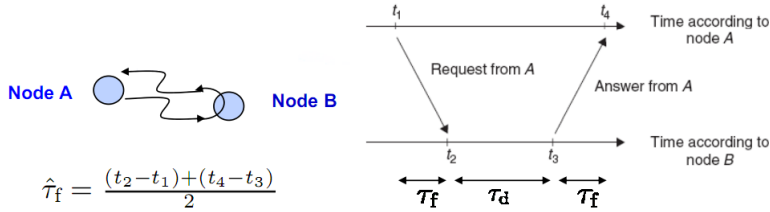
Figure 2.2: Example of One-Way ToA Ranging [2].

eliminated, clock drift still affects ranging accuracy, introducing significant error. In fact the propagation delay τ_f is typically in the order of nanoseconds, but the time response τ_d can be of some microseconds. During τ_d, thus, we can have an error accumulation due to clock offset between node A and B that leads to a bad ToA estimation and, consequently, a bad ranging calculation.

Time-Difference-of-Arrival [4][2]   This technique can be implemented in two different ways: in the first one multiple synchronized nodes (*anchors nodes* in our case readers) send signals to the *target node* (in our case tags). This target answers to every anchors and the anchors make a triangulation like GPS system. In the second way, instead, target node broadcasts a signal that will be collected by anchors. In both two methods the information on ToA collected by each node is shared, and TDoA is realized. Usually the anchors are connected by a network, and their positions are well known. The TDoA

can be see like an hyperbola and the intersection of at least three hyperbolas give the position of the target node.
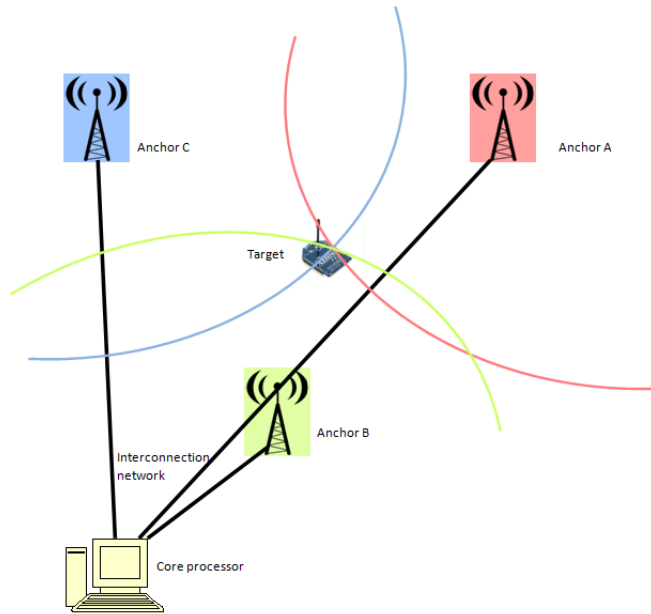
Figure 2.3: Example of TDoA Ranging.

2.2 Errors in Time-Based Ranging

2.2.1 NLOS propagation

When a signal propagates in the air, not always it travels through a direct path from transmitter to receiver, but it can encounter obstacles like walls, reflectors and so on, especially in an indoor environment. All these obstacles change the time-of-flight of the signal (usually increasing its value) making a distortion on ranging estimation.
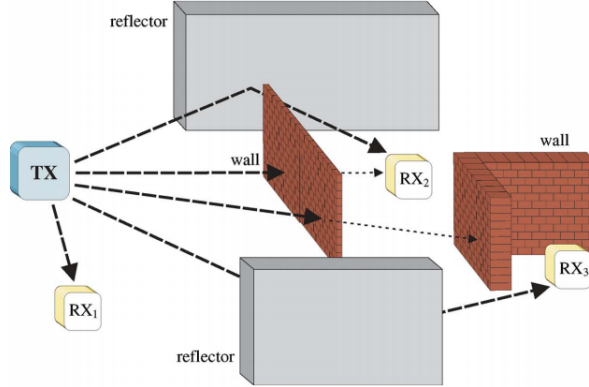
Figure 2.4: Example of LOS and NLOS propagation [4].

Multipath   Multipath propagation causes a phenomenon called *fading*. Fading is characterized by destructive and constructive interferences in the incoming signal at receiver side. The signal transmitted can travel through different paths (as shows in Fig. 2.4) and arrives in many replicas, each with its phase, that is added at receiver side generating a signal where the maximum may not correspond with the first path (see Fig. 2.5). Despite UWB signals can help in the resolution of the multipath problem; some environments make the detection of direct path not trivial.

Consider a scenario where $p(t)$ is a unitary energy pulse of duration T_P; at receiver side, in presence of multipath and thermal noise, we have:

$$r(t) = s(t) + n(t) \tag{2.2}$$

where $s(t)$ is the channel response to $p(t)$, and $n(t)$ is the Gaussian noise (AWGN) with two-side power spectral density $N_0/2$ [4].

In presence of frequency-selective channel we have:

$$s(t) = \sqrt{E_P} \sum_{l=1}^{L} \alpha_l p(t - \tau_l) + n(t) \tag{2.3}$$

where L is the number of multipath components with amplitude α_l and delay τ_l, E_P is the average received energy per pulse and we consider the normalization $\sum_{l=1}^{L} \mathbb{E}[\alpha_l^2] = 1$ [4] ($\mathbb{E}[\cdot]$ is the expectation of $\cdot$).
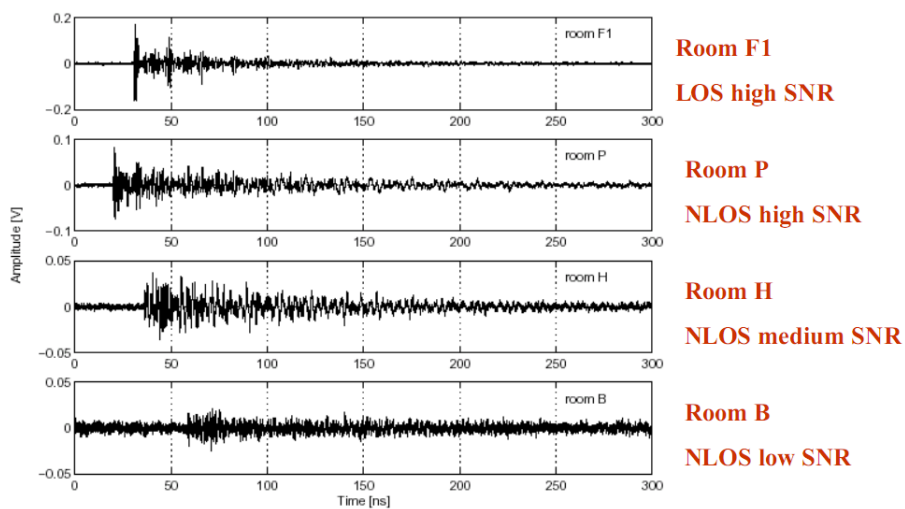
Figure 2.5: Example of LOS and NLOS signals with different SNR [9].

Excess Delay   Another source of error is the Direct Path (DP) excess delay. When the direct path from transmitter to receiver is obstructed by an object, the signal travels slower than it could do in air, causing an excess delay which affects ranging calculation. The excess delay can be computed as follows [4]

$$\triangle\tau = (\sqrt{\epsilon_r} - 1)\frac{d_W}{c} \qquad (2.4)$$

where ϵ_r is the relative electric permittivity of the obstacle, d_W the thickness material and c the light's speed. Recent experiments show that ranging error is on the order of wall's thickness between transmitter and receiver [5].

NLOS condition   When DP is totally obstructed, the signals comes to receiver by multiples reflected paths. In this way the path travelled is longer than DP, and the distance between transmitter and receiver is overestimated. We can model this error in ranging measurements like we have done for excess delay, because the delay introduced by NLOS paths is similar to delay due to wall penetration

in DP semi-obstruction.

Many techniques are proposed to mitigate this bias introduced by NLOS propagation, for example quadratic programming and linear programming approaches, or introducing memory in the system [4].

2.2.2 Clock Drift effects

As showed in Sec. 2.1, ToA estimation needs extremely precise measures of time intervals. In passive RFID context, readers are powered and usually can have more expensive hardware than tags; in this way their oscillators are precise enough for centimetre ranging accuracy. Separate speech can be done for tags; indeed, they usually result equipped with simple and low-cost hardware, and their oscillators can introduce a drift respect to real time t.

Consider $C(t)$ a function for the local time of the clock in a device; for short time intervals we can write [4]

$$C(t) = (1 + \delta)t + \mu \tag{2.5}$$

where δ is the *clock drift* with respect to the correct rate and μ is the *clock offset*.

Using (2.5) we can compute the estimated One-Way ToA as above [4]:

$$\begin{aligned}\hat{\tau}_f = C_B(t_2) - C_A(t_1) = \\ = \tau_f + \delta_B t_2 - \delta_A t_1 + \mu_B - \mu_A\end{aligned} \tag{2.6}$$

Eq. (2.6) shows how ToF estimation is affected both by clock drift and clock offset. Critical is the presence of clock offset, because usually it can have values on the order of microseconds; so the performance of One-Way ToA algorithm strictly depends on network synchronization accuracy.

Two-Way ToA algorithm eliminates clock offset in ToF estimation. In fact if the round-trip time estimated is [4]

$$\hat{\tau_{RT}} = 2\tau_f(1 + \delta_A) + \frac{\tau_d(1 + \delta_A)}{\delta_B} \tag{2.7}$$

and the round-trip time expected is

$$RTT = 2\hat{\tau}_f + \tau_d \tag{2.8}$$

we can equate (2.7) and (2.8) obtaining

$$\hat{\tau}_f = \tau_f(1 + \delta_a) + \frac{\varepsilon \tau_d}{2(1 + \delta_A - \varepsilon)} \qquad (2.9)$$

where $\varepsilon \triangleq \delta_A - \delta_B$ is the relative clock offset. In this way, the ranging error depends only on ε; so if we want to achieve high precision, good oscillators have to be present on tags hardware.

2.3   Theoretical limits for ToA estimation

If we consider the ToA estimation, we are interested in evaluating the first arriving path. Consider an observation period $[0; T_{ob})$, and a signal arriving with a delay uniformly distributed between 0 and T_a with $T_a < T_{ob}$. In ideal propagation conditions, received AWGN signal can be written as (2.3). Considering only the first path we have [4]

$$s(t) = \sqrt{E_P}p(t - \tau) + n(t) \qquad (2.10)$$

In this conditions, the ToA estimation becomes a classical non linear parameter estimation problem. The received signal is processed as reported in figure below. ToA corresponds to the maximum absolute
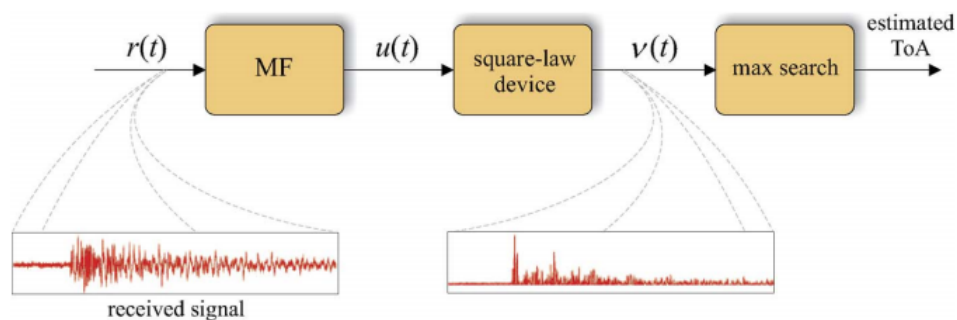
Figure 2.6: Example Processing chain at receiver side [2].

peak at the output of the Matched Filter (MF) inside the observation

interval.

This scheme can be seen as a ML estimator [4] in the case that the received signal is perfectly known, which is known to be asymptotically efficient. Indeed, in case of high SNR this maximum efficiency is given by the Cramer-Rao Bound (CRB). This gives the Mean Square Error (MSE) bound for any unbiased estimator of $\hat{\tau}$ and its expression is given by:

$$CRB = \frac{N_0/2}{(2\pi)^2 E_P \beta^2} = \frac{1}{8\pi^2 SNR \beta^2} \tag{2.11}$$

where (2.11) is known as CRB [4]. Signal to Noise Ration is

$$SNR = E_P/N_0$$

and the second moment of the spectrum $P(f)$ to $p(t)$ is

$$\beta^2 \triangleq \frac{\int_{-\infty}^{+\infty} f^2 |P(f)|^2 df}{\int_{-\infty}^{+\infty} |P(f)|^2 df}$$

The best accuracy reached by our estimator is given by (2.11) multiplied by the speed of light to convert the bound on delay estimation in the bound for distance estimation. (2.11) then becomes:

$$\mathbb{V}[\hat{d}] \geqslant \frac{c^2}{8\pi^2 SNR \beta^2} \tag{2.12}$$

where $\mathbb{V}[\hat{d}]$ is the variance of estimated distance. In (2.12) we can note the dependence on both the SNR and β^2; this means that a signal with high power and large spectrum improves the estimation performance. For this reason UWB signals have been chosen for ranging measurement in SELECT project.

Another bound used for ToA estimation performance is the Ziv-Zakai Bound. This bound can be preferred with respect to the CRB for medium and low SNRs; instead for high SNRs the performance are the same (as shows in Fig. 2.4). In case of multipath environment, CRB and ZZB can be rewritten. In particular, CRB for the specific case where $|\tau_i - \tau_j| \geqslant T_p \ \forall i \neq j$ (where τ_i and τ_j are the delays for
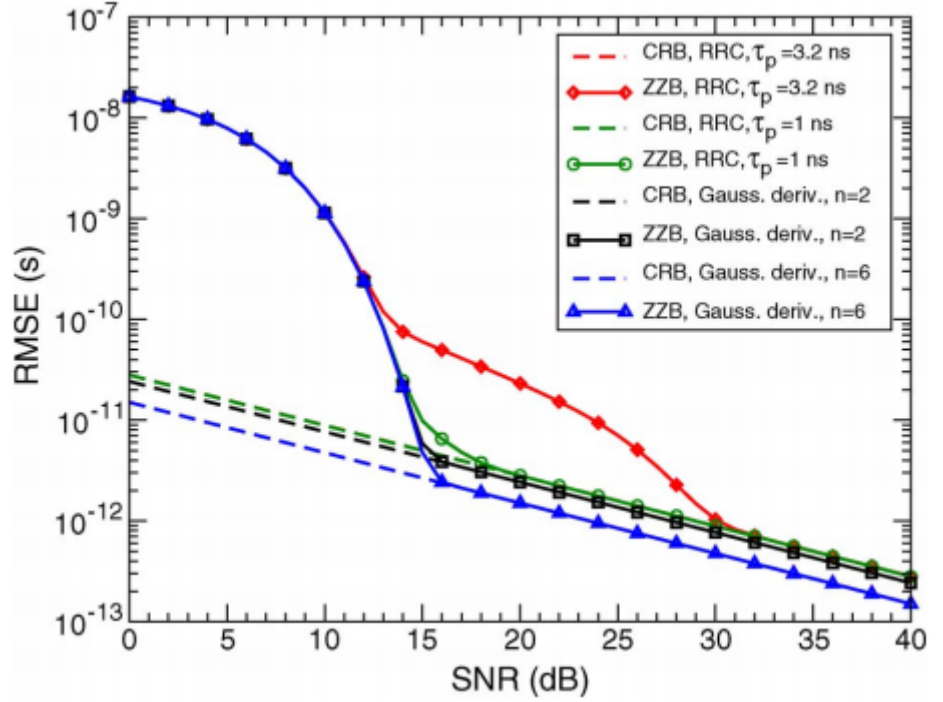
Figure 2.7: CRB and ZZB to the RMSE in function of different SNR in AWGN channel with $T_a = 100$ns. The second- and six-order Gaussian monocycle pulses with $\tau_p =0.192$, 1 and 32 ns as well as root raised cosine (RRC) bandpass pulses with $f_0 = 4$GHz, $\nu = 0.6$ are considered [4].

i-th and j-th paths and T_p is the pulse period) becomes [4]

$$CRB = \frac{N_0/2}{(2\pi)^2 E_P \beta^2} = \frac{1}{8\pi^2 SNR \beta^2 \alpha_1^2} \qquad (2.13)$$

α_1^2 represents the attenuation related to the first path (see (2.3)). Also in multipath case, a signal with high power and large spectrum improves the estimation performance.

Chapter 3

ToA estimation

3.1   classical ML estimation

The limits discussed in the previous chapter for the ToA estimation
can be reached, for high SNR, by the ML estimator. This estimator,
indeed, reaches the CRB in high SNR region, and it can be imple-
mented as a *Matched Filter* (MF), matched to the received signal.
The estimated ToA is equal to the delay that maximizes the output of
MF [4]. Unfortunately the receiver needs the estimation of the wave-
form received, and for this fact is difficult to implement this kind of
estimator. For this reason, ToA estimation in multipath environment
is closely related with channel estimation using ML approach [4].
In presence of AWGN channel (or with multipath but with Gaussian
noise), ML estimator is equivalent to MMSE criterion. Given an ob-
servation $r(t)$, we can derive ML estimation of ToA as [4]

$$\hat{\tau} = \ arg \ \max_{\tilde{\tau}}\{\chi^H(\tilde{\tau})R^{-1}(\tilde{\tau})\chi(\tilde{\tau})\} \tag{3.1}$$

where

$$\chi(\tau) \triangleq \int_0^{T_{ob}} r(t) \begin{bmatrix} p(t-\tau_1) \\ p(t-\tau_2) \\ \vdots \\ p(t-\tau_L) \end{bmatrix} dt \tag{3.2}$$

and $R(\tau)$ is the autocorrelation matrix of $p(t)$ with elements $R_{i,j} = \rho_P(\tau_i - \tau_j)$. In (3.1) χ^H represents the Hermitian adjunct (conjugate

transpose) of χ, and (3.2) is the correlation between the received signal and differently delayed replicas of the transmitted pulse [4]. When the channel is resolvable we can rewrite (3.1) as [4]:

$$\hat{\tau} = \ arg \ \max_{\tilde{\tau}} \left\{ \sum_{l=1}^{L} \left[\int_0^{T_{ob}} r(t)p(t - \tilde{\tau}_l)dt \right]^2 \right\} \qquad (3.3)$$

where L is the number of paths and $\tilde{\tau}_l$ is the delay associated to the l-th path. In this case, the delay of the first path is decoupled from the estimation of other channel parameters and only a single correlator is necessary, or a MF matched to the pulse $p(t)$ like happens in AWGN channel.

However, the difficulties in implementing the ML detector for real cases make necessary the adoption of suboptimal ToA estimators aimed at achieving ideal bound imposed by theory.

3.2   Practical ToA estimators

In literature there are a lot of suboptimal solutions proposed to obtain better ToA estimation. Some of them are reported in this section.
Usually, ML estimators work at Nyquist sampling rate, and the implementation is difficult to realize because the use of UWB signals characterized by high bandwidth. Suboptimal estimators analyzed in this section try to solve this problem working at sub-Nyquist rates. This is possible by introducing *Energy Detector* (ED) estimators, indeed this estimators make the ToA estimation not directly on the received signal, but on the energy profile obtained by dividing in slot the received signal along different time slots. ED-based ToA estimators can work with a particular signal structure born for multiple access, where a generic user u transmits a packet with a preamble [4]. The preamble (see Fig. 3.1) used for synchronization, acquisition and ranging is composed of N_{sym} symbols of duration T_s. Each symbol is an unmodulated TH (time hopping) signal divided in N_s frames of duration T_f. Each frame is in turn divided into N_c chips of duration T_c [4]. A unitary energy pulse $p(t)$ of duration $T_p < T_s$ is transmitted at each frame, and it is modulated according to a user-specific pseudorandom TH sequence having period N_S [4]. Thus, preamble

is composed of $N_t = N_{sym} \cdot N_s$ pulses. Typically, the ToA estimator
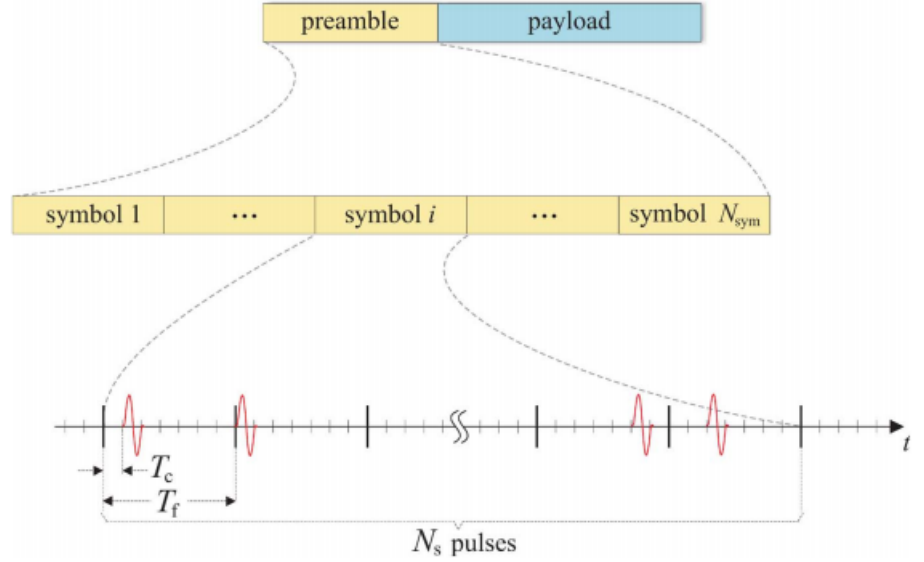
Figure 3.1: Example of preamble structure for ToA estimation [4].

is composed of four blocks as shown in Fig. 3.2. At first there is a
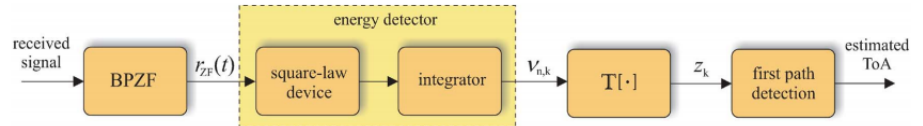
Figure 3.2: Example of processing chain for ToA estimation [4].

BandPass Zonal Filter with center frequency f_0 and bandwidth W to eliminate out-of-band noise. The out of this section can be written as:

$$r_{ZF}(t) = s_{ZF}(t) + i(t) + n(t) \tag{3.4}$$

where $s_{ZF}(t)$ is the channel response after BPZF at transmitted pulse $p(t)$, $i(t)$ is the interfering term and $n(t)$ is the thermal noise. The

input of ED block is composed of $r_{ZF}(t)$ divided in N_t subintervals each of duration $T_{ob} < T_f$. Each interval is sampled every T_{int} seconds, thus in a subinterval we have $K = \lfloor T_{ob}/T_{int} \rfloor$ samples. Now, the true ToA is contained in the time slot $n_{ToA} = \lfloor \tau/T_{int} \rfloor$ [4].

Assuming τ uniformly distributed in the period $[0; T_a)$ where $T_a < T_{ob}$, also n_{TOA} is uniformly distributed between 0 and $N_{ToA} - 1$ ($N_{ToA} = \lfloor T_a/T_{int} \rfloor$). It is important remember that n_{ToA} samples contain noise and possible interference, the following $n_{Toa} + 1$ contain the first path and the $K - n_{ToA} - 1$ contain noise, interference and echoes of useful signal. The time resolution of ED-based estimators is given by T_{int}, and the minimum achievable RMSE is:

$$RMSE_{min} = T_{int}/\sqrt{12} \tag{3.5}$$

After ED block, we can built a matrix $\mathbf{V}$ of $N_t \times K$ elements, each of them computes as [4]

$$\nu_{n,k} = \int_{kT_{int}}^{(k+1)T_{int}} |r_n(t)|^2 dt \tag{3.6}$$

where $n = 0, ..., N - 1$, $K = 0, ..., K - 1$ and $r_n(t)$ is portion of the received signal after dehopping in the n-th interval. Now applying a generic transformation $\mathbb{T}[\cdot]$ we produce a vector $\mathbf{z} = \{z_k\}$ used for ToA estimation. The conventional way to obtain $\mathbf{z}$ is to average along columns of $\mathbf{V}$ (*simple averaging*)

$$z_k = \sum_{n=0}^{N_t-1} \nu_{n,k} \tag{3.7}$$

with $k = 0, ..., K - 1$. The energy profile obtained, in Fig. 3.3 is reported; and above them, different ToA estimation techniques will be described and tested.

3.2.1   Dardari's method

The choice of the threshold η strongly influences the performance of ToA estimation. When η is small, we expect a high probability of early detection prior to the first path due to noise and interference. On the
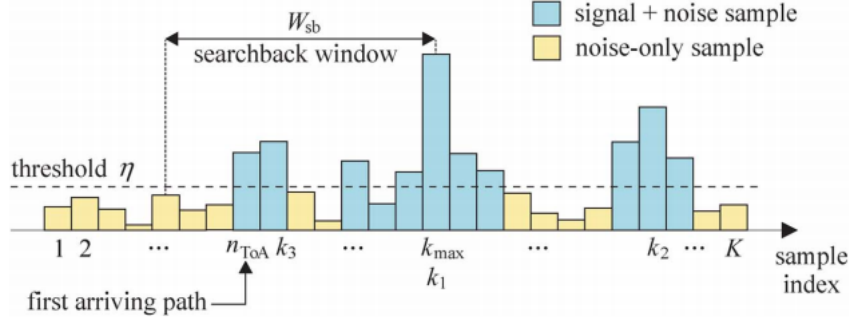
Figure 3.3: Example energy profile used for ToA estimation [4].

other hand, if η is large, we expect a low probability of detecting the first path and a high probability of detecting an erroneous path due to fading [4].

The early detection probability (P_{fa}) can be written introducing ξ in its expression as reported below [4].

$$P_{fa} = 1 + \frac{(1 - q_0)^{N_{TOA}} - 1}{N_{TOA} \cdot q_0} \tag{3.8}$$

where

$$q_0 \triangleq e^{-TNR} \sum_{i=0}^{M/2-1} \frac{TNR^i}{i!} \tag{3.9}$$

whit $TNR = \eta/N_0$ and $M = 2N_s T_{int} W$. N_0 is the noise power, N_s the number of symbols considered, T_{int} period of the integration window and W is the signal bandwidth.

Fixing a value for P_{fa} we can evaluate (3.8) and obtain a value for η. This method is unbound by the knowledge of the received signal characteristics, but does not lead to a significant performance degradation with respect to the optimal threshold described in Sec. 2.2.4.

3.2.2 Empirical method

An empirical method similar to the previous works imposing a fixed threshold over noise level, and make the ToA estimation with the value calculated (usually TNR is 1 or 2 dB). Obviously large values of threshold over the energy of the noise N_0 lead to little values of P_{fa}.
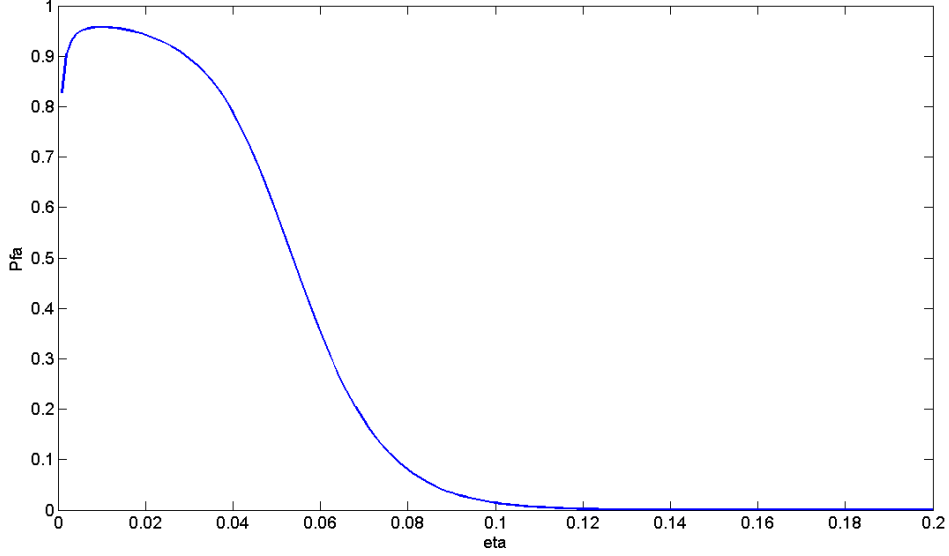
Figure 3.4: Example P_{fa} as a function of η calculated with (3.8) with $E_b/N_0 = -20$ dB, $T_{int} = 1.9$ ns, $N_s = 1$ and $W = 1$ GHz.

3.2.3   Guvenc's method

Another empirical method based on the energy of the noise can be used for the threshold setting. If μ_{ed} and σ_{ed}^2 are the mean and the variance of the noise samples that are at the output of the energy detector, the probability of erroneously interpreting a noise sample as a signal sample is [6]:

$$P_{fa} = Q(\frac{\eta - \mu_{ed}}{\sigma_{ed}}) \tag{3.10}$$

where $Q(\cdot)$ is the Gaussian Q-function, $\mu_{ed} = M\sigma_n^2$, $\sigma_{ed}^2 = 2M\sigma_n^4$ and $M = 2WT_p$ (T_p is sampling period) that depends by the signal bandwidth (imposed by the BPZF) and by the sampling rate. In (3.10) it has been assumed a Gaussian approximation of the Chi-square statistics, which is valid for large M, large processing gain or large N_{sym}. By fixing P_{fa}, the threshold can be calculated as:

$$\eta = \sigma_{ed}Q^{-1}(P_{fa}) + \mu_{ed} \tag{3.11}$$

Usually, in real environments, the UWB received signal arrives in clusters separated by noise-only samples. In this case, thus, with D consecutive noise samples considered, the P_{fa} becomes [6]:

$$P_{fa} = 1 - [1 - Q(\frac{\eta - \mu_{ed}}{\sigma_{ed}})]^K \qquad (3.12)$$

Thus the threshold for a fixed P_{fa} becomes [6]:

$$\eta = \sigma_{ed}Q^{-1}(1 - (1 - P_{fa})^{1/K}) + \mu_{ed} \qquad (3.13)$$

The parameter K is to be tuned for the channel model considered, and represents the number of bins between the one containing the first path and the bin with maximum energy.

3.2.4 Optimal thresholding

Usually to make the detection of the useful signal in the received waveform, a threshold applied to the energy profile is used; in particular, the ToA of the first path is estimated considering the first bin over the threshold (η). In literature, some different techniques to determine the best threshold are used, but none of them are better than *optimal threshold*.

The optimal threshold is evaluated knowing a-priory information on the signal received. To determine the best performance achievable from our estimators, a simulation with the *optimal thresholding* has been done. The a-priori information on the signal is the delay τ of the first path. By the knowing of this parameter, it is possible (tuning the threshold at the receiver side) makes the detection of the first path and, thus, estimates the correct ToA of the signal. The ToA estimation is done modifying the threshold until the ToA estimated is the same of the delay τ imposed at the signal during its generation. Obviously, this estimator works well only for the specific case for which the threshold has been evaluated, making it unsuitable for not scenario-specific applications.

3.2.5 Noise estimation

All the method reported above are based on a channel with AWGN noise with power spectral two-side density $N_0/2$. If is received a signal

composed only by noise $r(t) = n(t)$, every bin of energy at the output of our energy detector has got a "mean" (looking at many different realizations) energy value given by:

$$\sigma^2 = 2 \cdot N_0/2 \cdot W \cdot T_{int} \tag{3.14}$$

If the noise power is unknown, it is possible to estimate it as, for example, with an ML estimator.

Seen that we have a Gaussian noise modelled like a normal random variable (r.v.) $\mathcal{N} \sim (0, \sigma^2)$, the ML estimator in its unbiased version becomes [7]

$$\hat{\sigma^2} = \frac{1}{N-1} \sum_{i=1}^{N} (r_i - \hat{\mu})^2 \tag{3.15}$$

where $\hat{\sigma^2}$ is the noise power estimated, N is the number of the samples tested for the estimation, $\hat{\mu}$ is the estimated mean of the noise power and r_i are the samples received composed only by noise. This samples can be collected "listening" the channel when there are none transmissions.

3.3 Performance of practical ToA estimators

3.3.1 Simulator description

Before analyzing the performance of practical ToA estimators discussed in Sec. 3.2, it is necessary to describe how the algorithms have been implemented in our simulator.

First of all, the signals used in our test are composed of:

- 100 realizations of the 802.15.4a channel model

- root raised cosine (RRC) signal with $\beta = 0.6$ (roll-of factor), $f_0 = 3.95 GHz$ (central frequency), and $T_p = 1ns$ (pulse duration parameter)

All signals are normalized so that they have average unitary-energy, and at the receiver side we have an $SNR = 1/N_0$ that in dB is
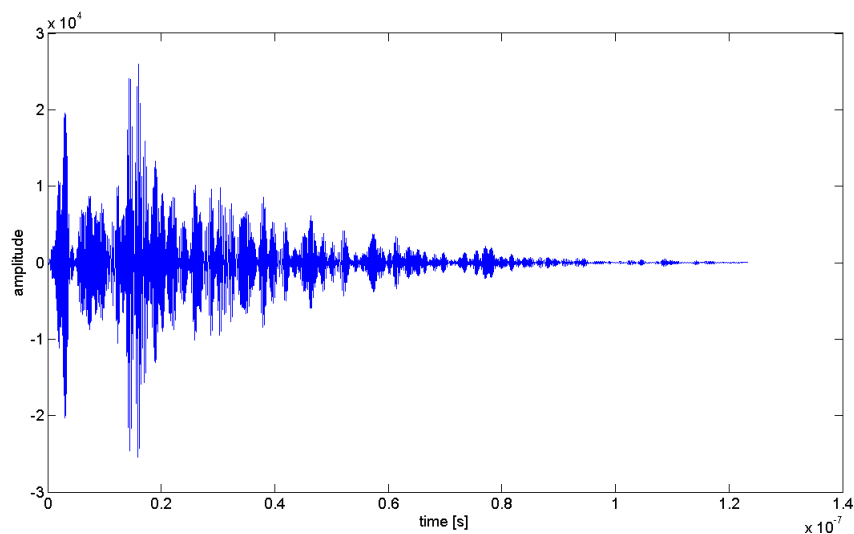
Figure 3.5: Example of signal with 802.15.4a channel model. First realization of the a hundred considered. 20dB of SNR, 9 ns of delay.

$SNR_{dB} = -N_{0_{dB}}$.

It is important to analyze the degradation of the performance when a signal propagates in real environment respect ideal propagation conditions (no multipath ad interferences).

The simulator built to test the performance of practical ToA estimators uses the Monte Carlo approach to examine all the possible scenarios for real propagation of the signals in the air. Starting with the signal from 802.15.4a channel model or AWGN model, a zero-padding and circular shift to reproduce the random ToA a have been done to fit the specifications of Sec. 3.2. The new signal has got a 152 ns of duration and a delay generated as a uniform r.v. between 0 and 30 ns. In particular, the delay can be seen as the value τ related to the ToA of the first path, and in this way the value to estimate. After the delay generation, to recreate real propagation of a signal in the air, a noise has been generated and added to our signal. Noise in our case is AWGN with power spectral density $N_{0_{dB}} = -SNR_{dB}$.

Now, the signal thus generated can be seen as the signal $r(t)$ (after the BPZF) at the input of the processing chain of Fig. 3.2 at the receiver
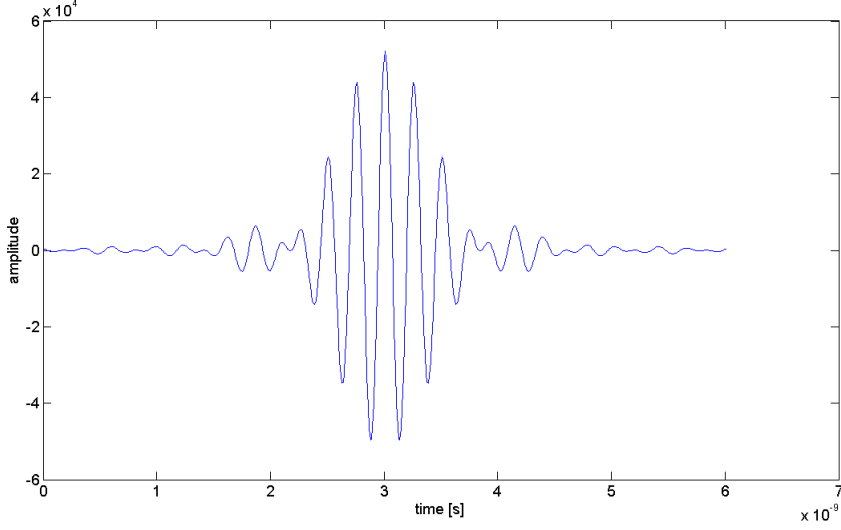
Figure 3.6: Example of the RRC signal with SNR=20dB and delay of 29 ns

side.   The core of processing chain is the energy detector. This block can be seen as (3.6), but in our case we have a time-discrete signal composed of $N_{samples} = 152ns/dt = 15200$ samples (where $dt = 1 \cdot 10^{-11}$ is the sampling period); so (3.6) can be rewritten as:

$$z_k = \sum_{i=1}^{N_{T_{int}}} |r_i|^2 \cdot dt \tag{3.16}$$

where block $\mathbb{T}[\cdot]$ of the processing chain has been enclosed in energy detector. $N_{T_{int}}$ represents the number of samples per integration period, r_i the i-th received samples and z_k the k-th energy bin.   On the energy profile obtained for every realization, we can apply the threshold calculated as proposed in Sec. 3.2. In this way, we can estimates the delay $\hat{\tau}$ of the first path and compare it with the real delay τ generated has a r.v. . To analyze the performance the *root mean square error* (RMSE) can be used.
If $\epsilon = \tau - \hat{\tau}$ is the error between the real delay and the estimated; the

26
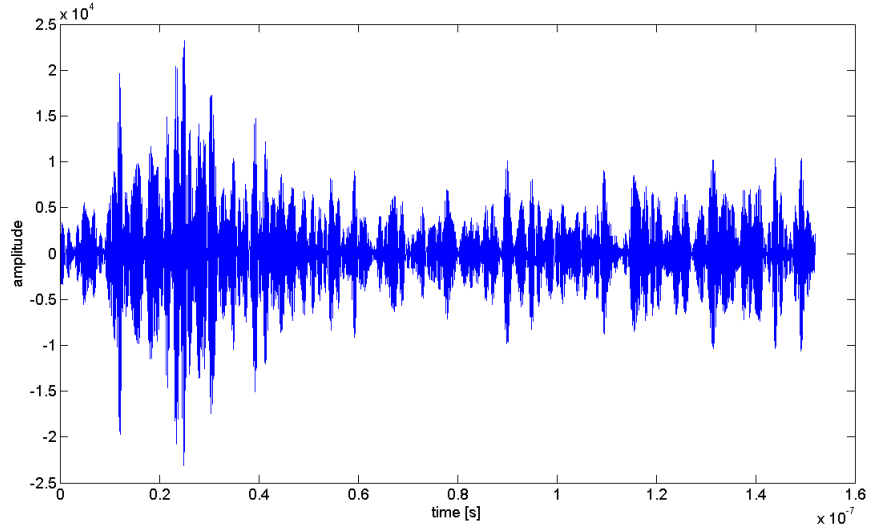
Figure 3.7: First realization of the a hundred considered signals for 802.15.4a channel model. In this case SNR=20dB and the delay generated is 9 ns.

mean square error (MSE) can be written as:

$$MSE = \frac{1}{M \cdot N_r} \cdot \sum_{j=1}^{M} \sum_{k=1}^{N_r} \epsilon_{j,k}^2 \qquad (3.17)$$

where M is the number of Monte Carlo iteration, N_r is the number of channel realizations for 802.15.4a channel model, and $\epsilon_{j,k}$ is the error associated at the j-th Monte Carlo iteration of the k-th channel realization.
The RMSE is thus:

$$RMSE = \sqrt{MSE} \qquad (3.18)$$

For the AWGN channel model (3.17) can be written as:

$$MSE = \frac{1}{M} \cdot \sum_{j=1}^{M} \epsilon_j^2 \qquad (3.19)$$

because we generate only a signal, and we haven't a hundred channel realizations. To have the same statistics, thus, it is necessary increase
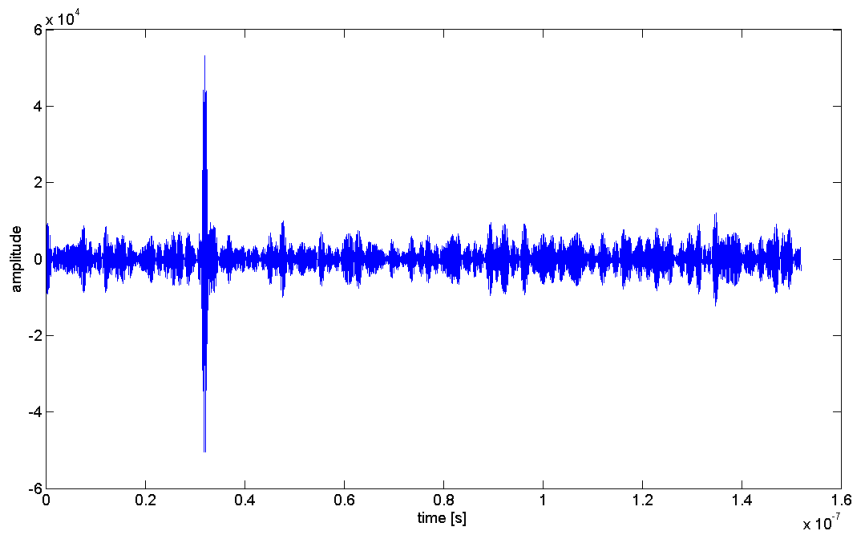
Figure 3.8: Example of received signal for AWGN channel model. In this case SNR=20dB and the delay generated is 29 ns.
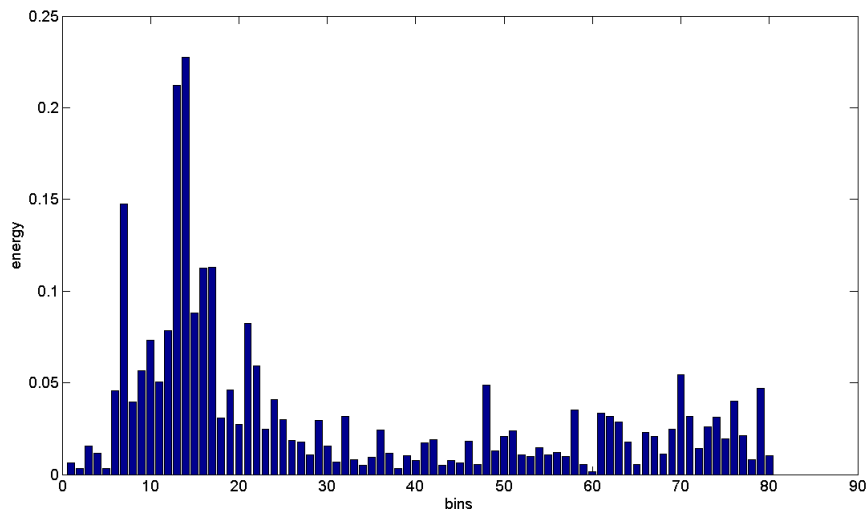
Figure 3.9: Energy profile of the signal of Fig. 3.7.
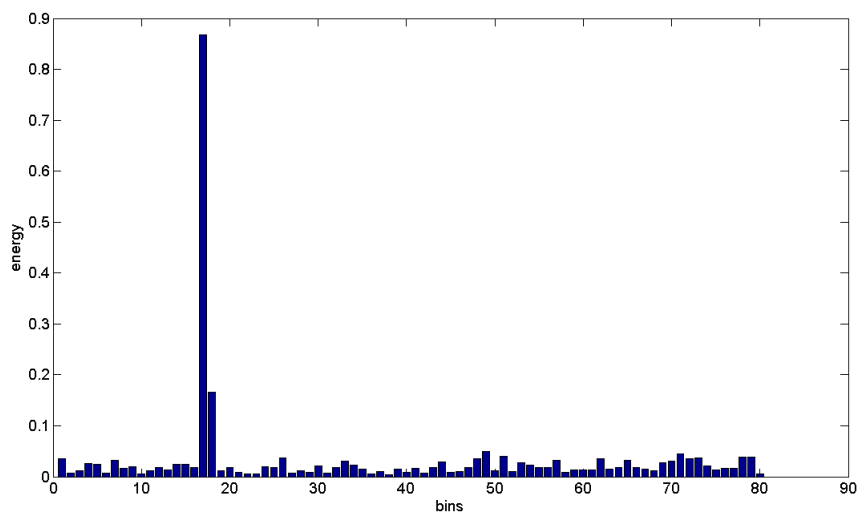
Figure 3.10: Energy profile of the signal of Fig. 3.8.

Monte Carlo iterations by a hundred factor.

3.3.2 Performance analysis and numerical results

The performance of the algorithm proposed in (3.2) will be evaluated
for the two kinds of signals described in (3.3.1). In particular the signal
used in 802.15.4a channel model were obtained for CM4, a channel
model to emulate a real propagation scenario. However the difference
between AWGN channel model and CM4 is that the SNR in AWGN
case refers to the energy concentrated in only one path, instead in
CM4 case the energy same energy is distributed in all paths received.

802.15.4a channel model

Optimal threshold The first algorithm tested is the optimal
thresholding. This algorithm aims to reach the best performance in
ToA estimation given by (3.5). In tested cases, $T_{int} = 2$ ns, so the
floor is 0.577 ns. As can be seen in Fig. 3.11, the floor is reached;
unluckily this floor is reached for high SNRs (up to 40dB), so in real
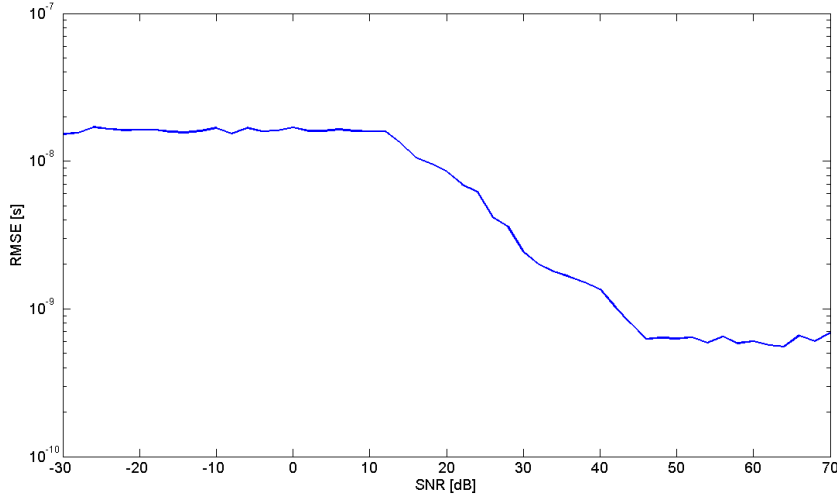
Figure 3.11: Performance of the *optimal thresholding* algorithm for different SNRs with CM4. 1000 Monte Carlo iterations, $N_s = 1$.

environments, to have good ranging performance, we have to work in optimal conditions or with high SNRs.

Dardari's method   With the threshold described in Sec. 3.2.1, the ToA estimated should be less good than the estimation obtained with the optimal threshold because this is a sub-optimal method. In Fig. 3.12 the performance are reported. As expected, the performance of this algorithm are worse than the optimal thresholding case, but it is not to be discarded.

Empirical method   By imposing the threshold some dB over the noise level, we can obtain not optimal performance like in the previous method, but the floor reached by this method is near to the theoretical one. As it can be seen in Fig. 3.13 the performance is very similar to the simple threshold with a precise P_{fa}.

Guvenc's method   The last method tested is that one reported in Sec. 3.2.3. In this case, the threshold is imposed after the obser-
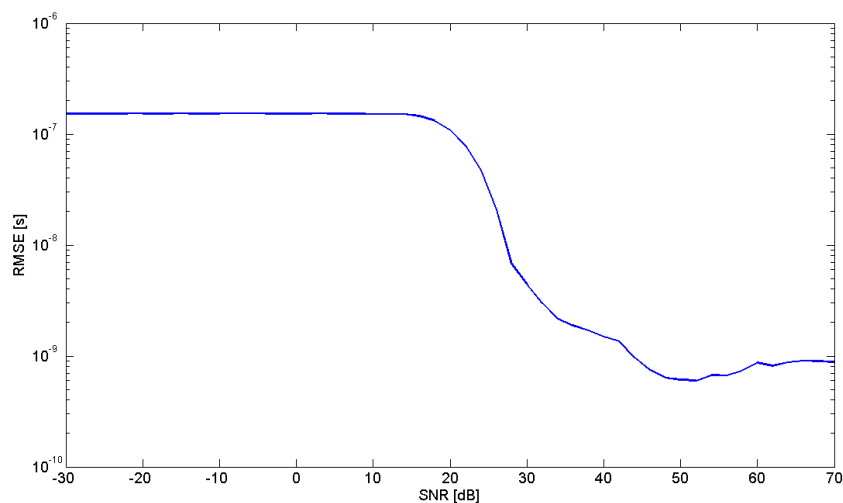
Figure 3.12: Performance of the *Dardari's method* algorithm for different SNRs with CM4. 2000 Monte Carlo iterations, $N_s = 1$ and $P_{fa} = 0.001$.

vation of the noise presents in the channel because to evaluate some parameters useful for a correct tuning of the threshold. The possibility to evaluate the threshold dynamically for every signal analyzed nominates this method to be the first for real time applications. The value taken for parameter K is 7 directly derived by simulations [6]. The performance is reported in Fig. 3.14. Nonetheless the performance not so good, thus this method is not suitable for precise ToA estimation.

A possible improvement to have better performance is to evaluate the mean value and the standard deviation of the noise above a received signal composed only by noise. Also many different signals composed only by noise can be received, so the statistic of the noise can be closer to reality.

AWGN channel model

Optimal threshold   As for 802.15.4a channel model, an analysis of the performance for AWGN channel model has been done (Fig.
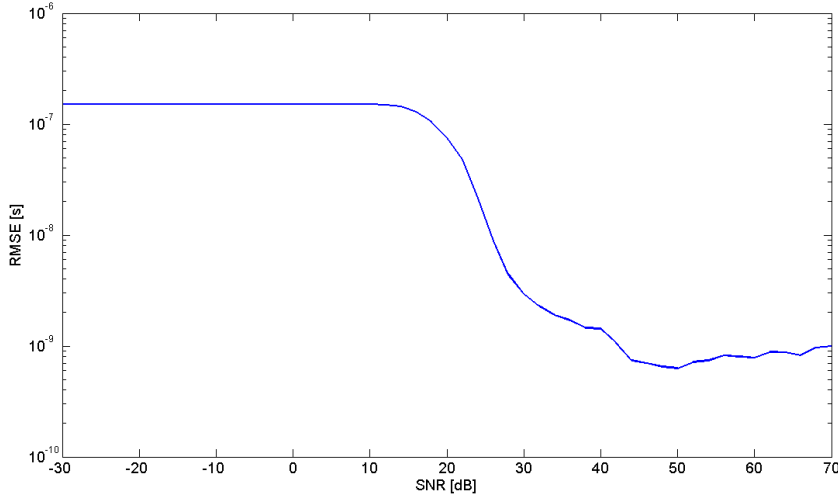
Figure 3.13: Performance of the *empirical method* algorithm for different SNRs with CM4. 100 Monte Carlo iterations and 8 dB over the noise level. It has been chose 8 dB because ensures the best performance looking different TNRs. $N_s = 1$.

3.15). The first algorithm tested is the optimal threshold. Also in this case we have to reach the floor of $T_{int}/\sqrt{12}$. The floor is not totally reached, indeed the minimum value is about of 0.68 ns (0.1 ns over the ideal floor). This appear not logical because the optimal threshold must reach the theoretical floor, but probably some approximations in the simulations generate errors that make impossible reach the ideal floor.

Dardari's method   Fixing a value for P_{fa} (0.001 in our simulations), the optimal value for the performance is reached for SNR=48 dB as shown in Fig. 3.16. Like for CM4 signals, this method is pseudo-optimal, and ensure a good trade-off between performance and ease of implementation, because not a-priory informations are required.

Empirical method   The empirical method applied to AWGN channel model (Fig. 3.17) gives the same results obtained in CM4
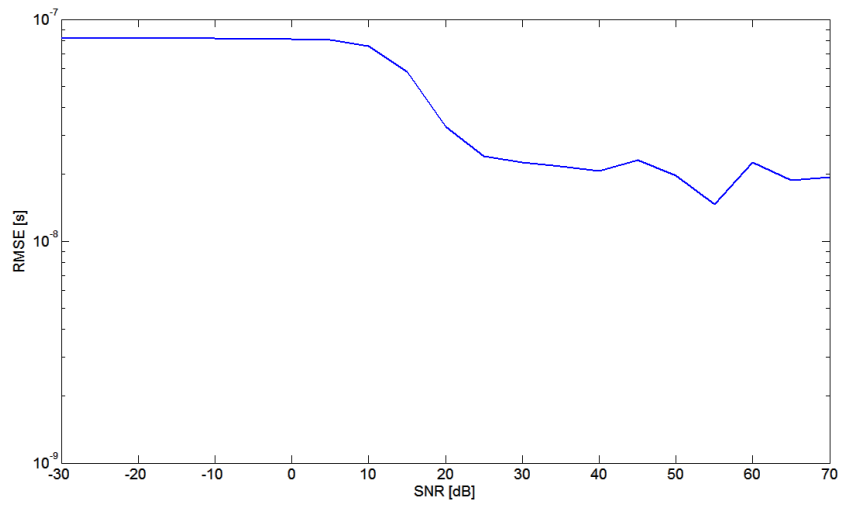
Figure 3.14: Performance of the *Guvenc's method* algorithm for different SNRs with CM4. 100 Monte Carlo iterations and $N_s = 1$.
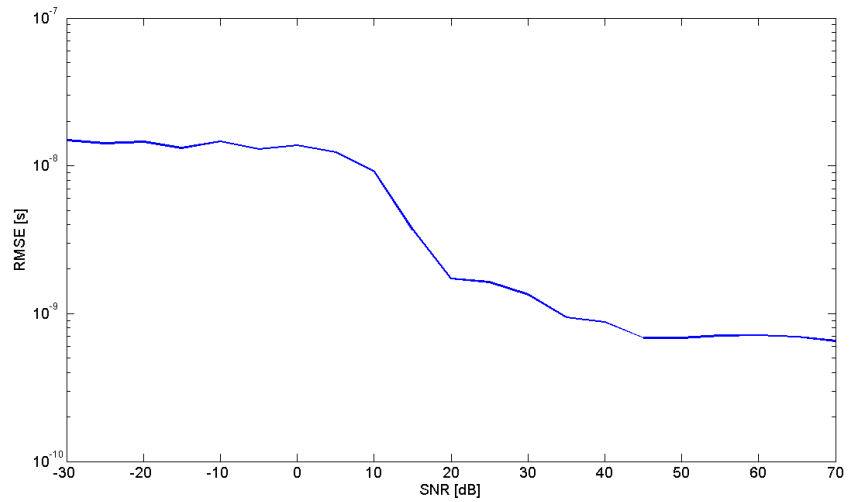
Figure 3.15: Performance of the *optimal thresholding* algorithm for different SNRs with AWGN channel model. 10 Monte Carlo iterations and $N_s = 1$.
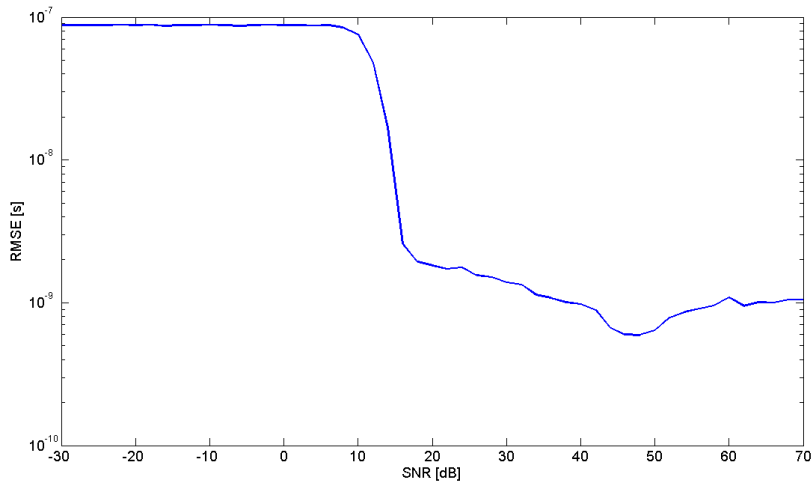
Figure 3.16: Performance of the *Dardari's method* algorithm for different SNRs with AWGN channel model. 2000 Monte Carlo iterations and $N_s = 1$.

with the same TNR (8 dB). This confirms the good behaviour both ideal conditions, both in real conditions.

Guvenc's method The last method tested also with AWGN channel model is the one described in Sec. 3.2.4. In this case, the parameter K is taken as 1 because there isn't multipath propagation, and the signal starts in the maximum energy bin, or very near it. In Fig. 3.18 the performance is reported. As it can be seen, the floor is about 2 ns; this can be explained considering that the signal starts in bin with low energy (see Fig. 3.6 to remember the signal) and the threshold is pulled up by the bins with maximum energy.
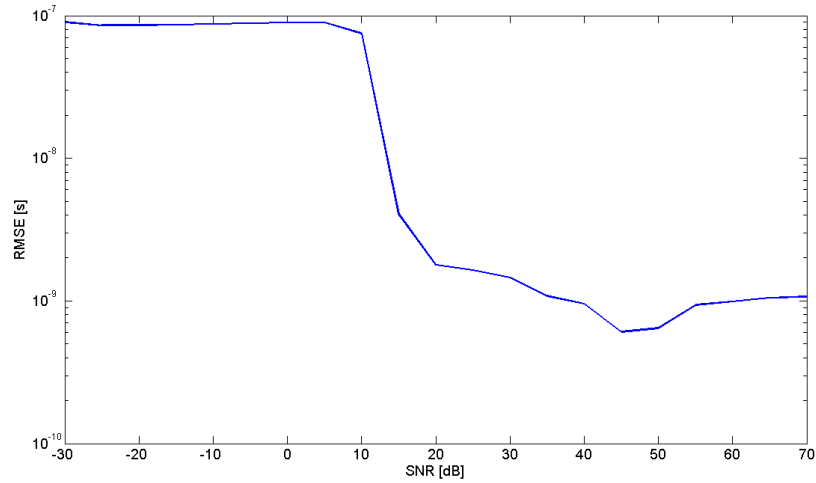
Figure 3.17: Performance of the *Empirical method* algorithm for different SNRs with AWGN channel model. 1000 Monte Carlo iterations and 8 dB over the noise level. $N_s = 1$.

3.3.3 Performance comparison

802.15.4a channel model

To understand which of the methods tested is the best or the worst, a comparison can be done. In Fig. 3.19 a curve, for each algorithm tested is reported. As it can be seen, *Optimal thresholding* reaches the best performance (as expected); instead *Simple thresholding with early detection imposition* and *Empirical method* have got the same performance, with favourite *Empirical method* because reaches the floor two or three dB before *Dardari's method*. *Guvenc's method* has got the worst performance, so this algorithm needs of some corrections to work well with CM4.

AWGN channel model

Also for AWGN channel model we propose a performance comparison. In this case (Fig. 3.20) the *optimal thresholding* is very closer to the floor for high SNRs that however it is not reached probably
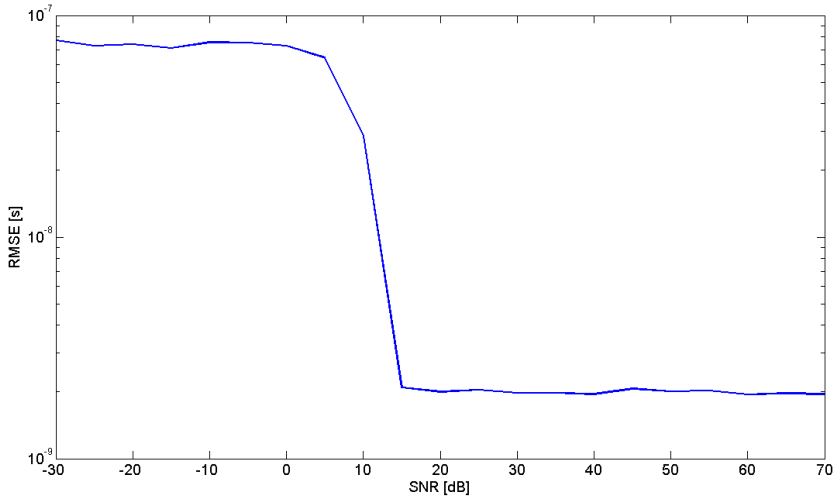
Figure 3.18: Performance of the *Guvenc's method* algorithm for different SNRs with AWGN channel model. 1000 Monte Carlo iterations and K=1. $N_s = 1$.

for motivation reported above; overall the performance is not so far from theoretical. For the other algorithm, instead we can conclude that below 15 dB of SNR *Guvenc's method* is to be preferred, while above 15 dB *Dardari's method* and *Empirical method* ensure the same performance.

We can conclude that there is full agreement between the results related at CM4 and AWGN channel model. This suggests that the algorithms tested don't significantly degrade their performance if applied in a real environment with the only exception for *Guvenc's method* that dramatically degrades its performance. Note that for low SNRs (both in CM4 both in AWGN channel model) the *optimal thresholding* has got better performance than the other methods. This can be explained because with other methods, when there is a lot of noise, the decision on the first path is uniformly distributed along the entire length of the signal; instead, with *optimal thresholding* probably the estimation is not random, but the optimal threshold may drive to better performance also in low SNRs' region.
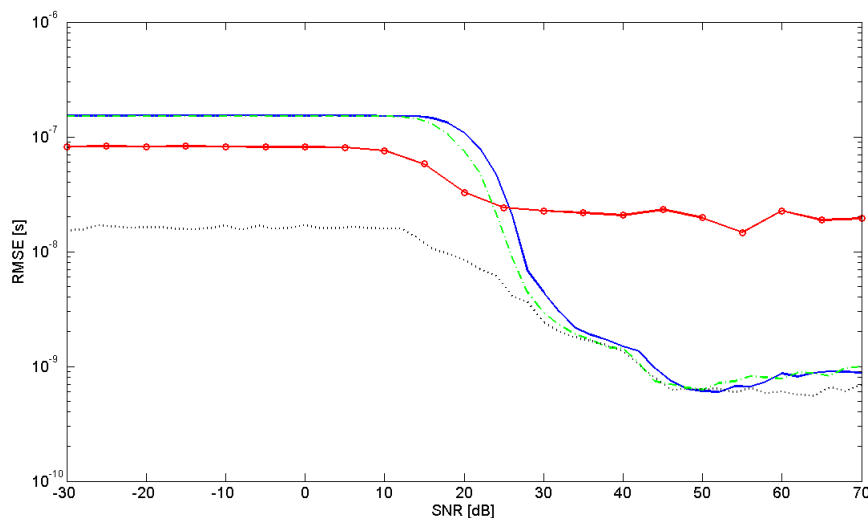
Figure 3.19: Performance comparison for CM4. In blu (solid line) *Dardari's method*, in black (dotted line) *Optimal thresholding*, in red ('o' line) *Guvenc's method* and in green (dashed line) *Empirical method* are reported.

3.3.4 Improving the performance for low SNRs

The algorithms reported in Sec. 3.2 present a problem: they have a good performance only at high SNRs. In ideal conditions, if we want a good ToA estimation, we have to choose one of the algorithm reported above, look at its performance, and work with the SNR that fits our requirements. If we look the plots reported above, we realize that the requirements on ToA estimation impose to work over 30 dB of SNRs. Unluckily, in SELECT we have to work with at most 15 dB of SNR. This constraint lead us to introduce a technique to reach good performance at SNRs indicated by SELECT project.

If the channel has been estimated by observing a single bit transmitted, we have had the performance reported in Sec. 3.3.2. To have better performance at low SNRs, the key idea is to improve the SNR by observing more than one bit for the ToA estimation. Accumulating the received bits and summing up together before the energy profile computation, we obtain a cumulative energy profile without peaks of
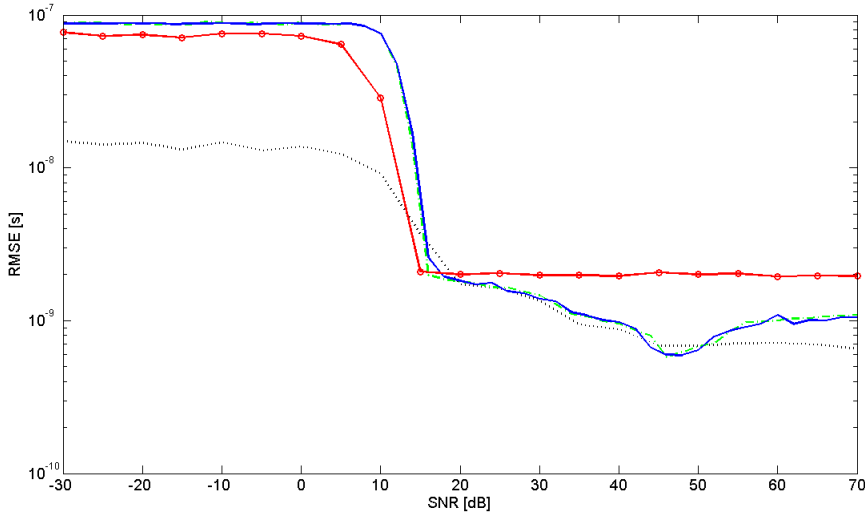
Figure 3.20: Performance comparison for AWGN channel model. In blu (solid line) *Dardari's method*, in black (dotted line) *Optimal thresholding*, in red ('o' line) *Guvenc's method* and in green (dashed line) *Empirical method* are reported.

noise present in one observation. Observing N realizations (where $N \to \infty$) we obtain, for bins with only noise, the value of the variance of the noise $N_0/2$.

As it can be seen in Fig. 3.21, 3.22 and 3.23, by observing more than one bit to build the energy profile, the noise forms a floor, so the signal is clearly identified and the algorithm can make a better ToA estimation also with low SNRs. An example of the performance improvement in Fig. 3.24, 3.25, 3.26 and 3.27 is reported. With *Optimal thresholding* and *Guvenc's method* we can see as the performance improve of some dBs in the transition region, reaching the floor at SNR's values closer at SELECT specifications. In the other two case, instead, we doesn't obtain significant performance improvement because of an incorrect parameter tuning. For example 8 dB over the noise level in *empirical method* case became too large for an high number of bits observed.

Obviously the observation of more than one bit can be exploited
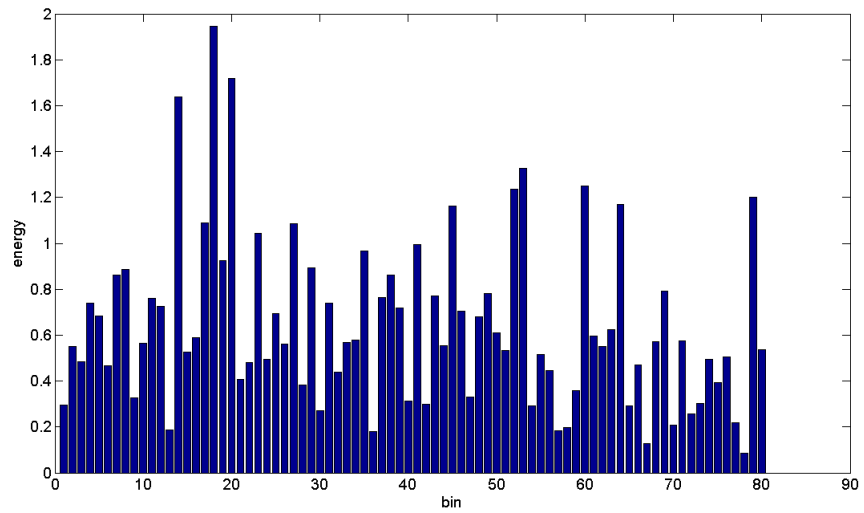
Figure 3.21: Energy profile for AWGN channel model with SNR=5 dB and 1 bit observed.
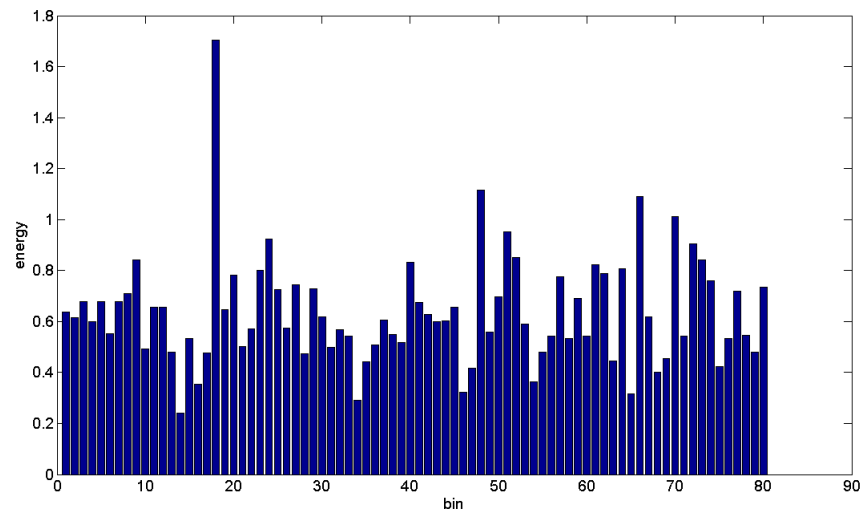
Figure 3.22: Energy profile for AWGN channel model with SNR=5 dB and 5 bit observed.
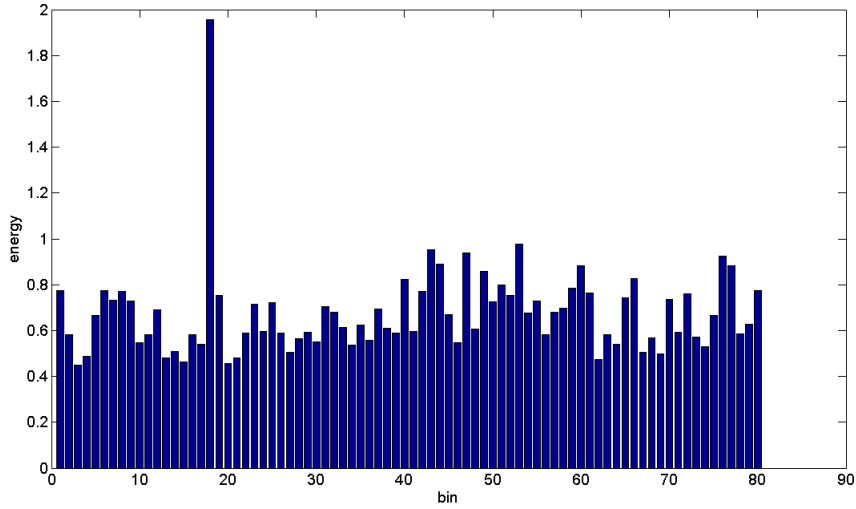
Figure 3.23: Energy profile for AWGN channel model with SNR=5 dB and 10 bit observed.

whereas a perfect synchronization may be done. In fact, if the aren't able to synchronize the receiver with each bit, we risk that the samples summed at the accumulation stage aren't perfectly overlapped compromising the correct ToA estimation.

Another constraint for the usage of this method is the time-stability of the channel. In fact if the channel changes between the first and the last bit sent, the bits received are not the same, so we meet the same problem reported above: the accumulation of different signals, that compromises the ToA estimation. Thus, we can conclude that the observation of more than one bit at receiver side to improve the SNR it is possible with good time synchronization at receiver side, and the number of bits observed are to be evaluated case by case depending by the time-stability of the channel. For SELECT scenarios a reasonable number of bits observed is 5. Over this value, the errors due to synchronization stage may be dangerous for the purpose.
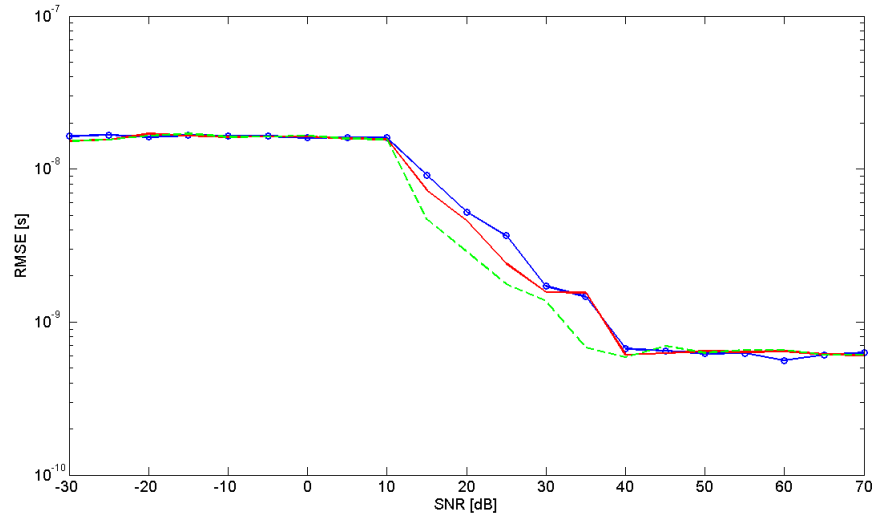
Figure 3.24: Performance for *Optimal thresholding* method and CM4 with 5 ('o' blue line), 10 (solid red line) and 50 (dashed green line) bits observed. 20 Monte Carlo iteration.

3.4 Method for improved ToA estimation

3.4.1 Overlapping the integration windows

To improve the performance of our estimator (lowering the floor for high SNRs) a possible solution may be the partially overlapping of the integration windows in the energy detection stage.

In a scenario where the integration windows are of 2 ns, if we overlap each integration window, we obtain an energy profile with the number of bins doubled (Fig. 3.28), and thus, the temporal resolution doubles. In this way we have a "virtual" $T_{int} = 1$ ns, so the floor becomes 0.29 ns. The performance with this method in Fig. 3.29 is reported.
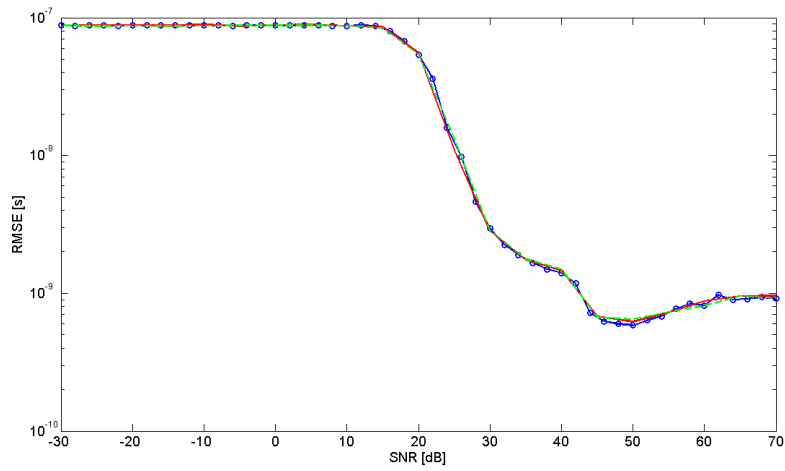
Figure 3.25: Performance for *Simple thresholding with early detection imposition* method and CM4 with 5 ('o' blue line), 10 (solid red line) and 50 (dashed green line) bits observed. 20 Monte Carlo iteration.
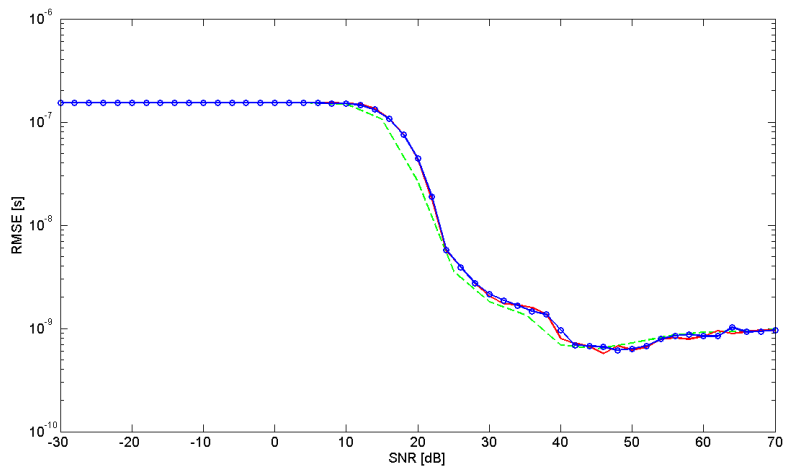
Figure 3.26: Performance for *Empirical method* method and CM4 with 5 ('o' blue line), 10 (solid red line) and 50 (dashed green line) bits observed. 20 Monte Carlo iteration.
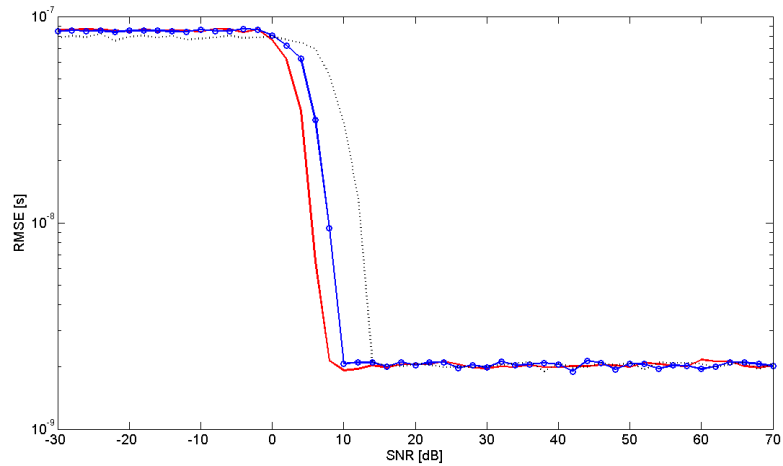
Figure 3.27: Performance for *Guvenc's method* and AWGN channel model method with 1 (dotted black line), 5 (solid red line) and 10 ('o' blue line) bits observed. 1000 Monte Carlo iteration.
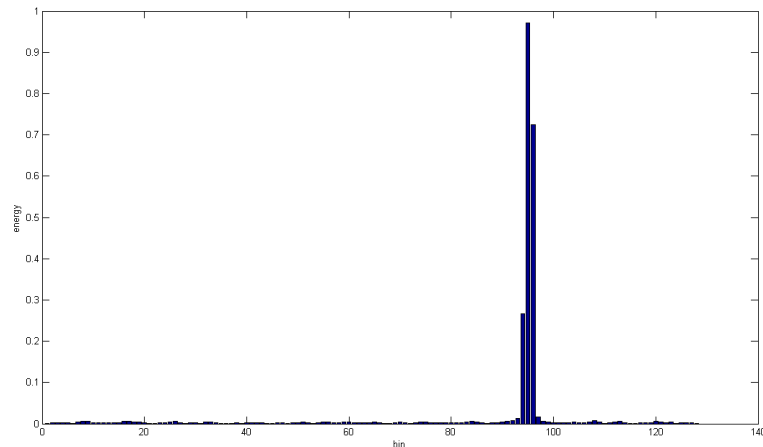
Figure 3.28: Energy profile in case of integration window 50% overlapped. $SNR = 30$ dB.

3.4.2 Maximum Likelihood estimation for unknown waveform

Theoretical basis

Another method for the ToA estimation, is the one which uses the Maximum Likelihood estimation (ML). This estimator works differ-
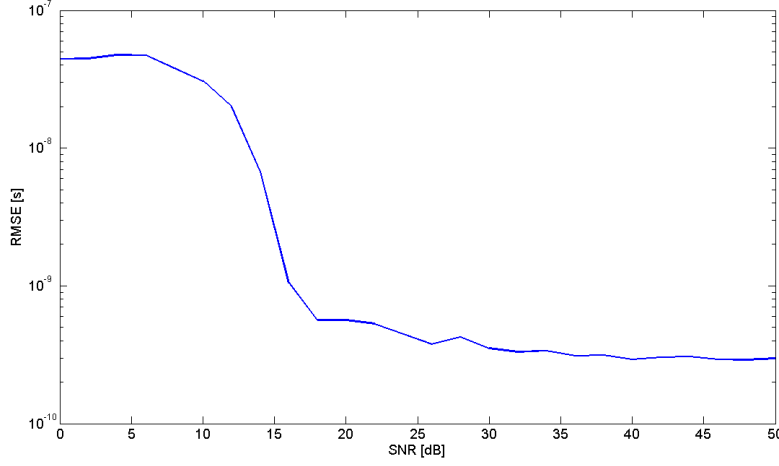
Figure 3.29: Performance of the *optimal thresholding* method applied to the energy profile with overlapping of the integration windows. 1000 Monte Carlo iterations and $N_s = 1$.

ently respect the estimators described in the previous sections, because none threshold is applied.

If we consider the usual received signal $r(t) = s(t - \tau) + n(t)$ (where τ is the unknown delay of the signal), the single sample received after the sampling stage can be written as $r_n = s_n + n_n$ where $r_n = r(n\mathrm{dt})$, $s_n = s(n\mathrm{dt})$ and $n_n = n(n\mathrm{dt})$ and dt is the sampling period according to Shannon-Nyquist.

Now, the **likelihood function** is:

$$\Lambda(r, s, \tau) = \beta \; exp \left\{ -\frac{1}{2N_0W} \sum_{n=1}^{N} (r_n - s_n)^2 \right\} \qquad (3.20)$$

where W is the bandwidth of the signal, N_0 is the noise power and β is an arbitrary constant not important for finding the maximum of the function. (3.20) is valid for $dt = 1/2W$. Therefore (3.20) is maximized in 2 steps:

1. find the estimate $\hat{s}$ of s that maximize 3.20 for every value of τ;

2. maximize with respect to τ.

Analytically:

$$\hat{\tau} = \; arg \; \max_{\tau} \; log\Lambda(r; t; s = \hat{s}) \tag{3.21}$$

where

$$\hat{s_n} = \begin{cases} r_n & if \; n \in \mathcal{D}(\tau) \\ 0 & elsewhere \end{cases} \tag{3.22}$$

and

$$\mathcal{D}(\tau) = \{k, k+1, \cdots, k + \lfloor T_p/dt \rfloor\}, \quad k = \lfloor \tau/dt \rfloor \tag{3.23}$$

T_p is the time duration of the transmitted signal (the only parameter of $s(t)$ known). Finally the ToA estimated is given by:

$$\hat{\tau} = \; arg \; \max_{\tau} \; \int_{\tau}^{\tau + T_p} r^2(t) dt \tag{3.24}$$

The one just written is the ML estimation for ToA arrival estimation of an unknown signal.

Implementation and performance

To implement this method of ToA estimation, it has been used the simulator analyzed in Sec. 3.3.1 with some changes specifics for this algorithm. In particular the last step of energy detection has been modified. While in the previous algorithm we applied a threshold over an energy profile of the received signal, now we build an energy profile by fixing an integration window of $T_{int} = 2$ ns and moving this window along the received signal sample by sample. In this way we obtain an energy profile as reported in Fig. 3.30.

With the energy profile of Fig. 3.30, the ToA estimation becomes the choice for the bin that maximizes the energy without the need of defining a threshold. In this way, for high SNRs there is the possibility to make the best ToA estimation. The performance of ML estimator for different T_{int} in AWGN channel have been investigated. The results are plotted in Fig. 3.31.

First of all in Fig. 3.31 we can note that some lines of performance are interrupted before 60 dB of SNR. This is not an error on the simulations, but seen that we use a logarithmic scale for y axes, the
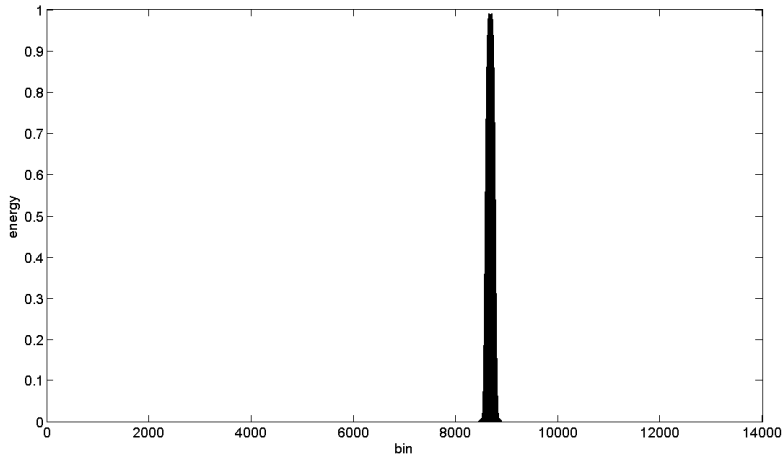
Figure 3.30: Energy profile with ML estimator at 60 dB of SNR.$T_p = 1$ ns, $T_{int} = 2$ ns and $N_s = 1$.

value 0 is not represented. Probably, This behaviour is due to the discretization of the delay introduced for the simulations to reproduce the propagation effects. The floor expected in case of no-discretized delay is of $dt/\sqrt{12} = 2.9$ ps. Second there is a floor on the performance for $T_{int} = 2$ ns. This may be explained if we expand the energy profile around the maximum (Fig. 3.32).

From Fig. 3.32 we note that there is not only a peak correspondent to the max, but there are two peaks symmetrical with respect to the max. Choosing for one of this 2 relative peaks, we don't make the correct detection of the real delay of the signal. This introduces a bias on the ToA estimation performance of $T_d/2 = 0.25$ ns (where T_d is the time distance between the two relative peak).

A probably explanation for an energy profile like the one of Fig. 3.32 can be found looking at the received waveform, in particular at the square of each samples, because they will be used for the energy profile construction.

In Fig. 3.33 we can see that the energy of the signal does not have a monotone profile, but we have 2 tails with part of the energy of the signal divided by the body that contains the maximum energy by 2 areas without energy. If an integration window of appropriates
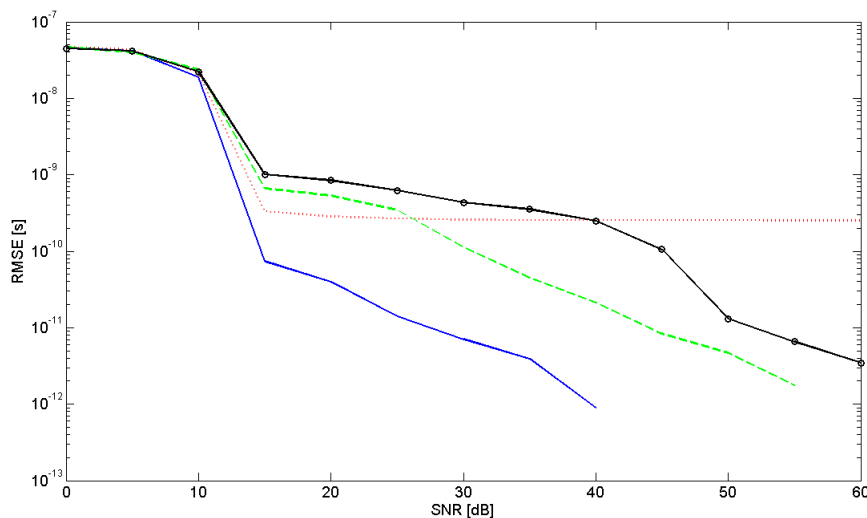
Figure 3.31: Performance comparison with ML estimator on AWGN channel for $T_p = 1$ ns. In blue solid line $T_{int} = 1$ ns, in red dotted line $T_{int} = 2$ ns, in green dashed line $T_{int} = 3$ ns and 'o' black line $T_{int} = 4$ ns. $N_s = 1$.

width makes a sweep along the signal, may assumes time positions which includes one tail and a large part of the body of the signal. When the integration window is perfectly centred over the body of the signal, instead, we do not consider the tails but we consider the areas without energy, so the energy profile has not the maximum energy on the center because discards the energy of the tails. This behaviour is present only with some values of T_{int} and changes if we consider different pulse duration. For $T_p = 1.6$ ns indeed we have the same problem at the energy profile for $T_{int} = 3$ ns, and on contrary if the signal reduces its duration (for example with $T_p = 0.8$ ns) we have no problem also with $T_{int} = 1$ ns, because every integration window includes always great part of the signal.

An example of how the tails modify their position with different value of T_p in Fig. 3.34 are reported in Fig. 3.35 where we can see that the floor for a signal with $T_p = 1.6$ ns is another time given by $T_d/2 = 0.35$ ns and this problem afflicts the performance for $T_{int} = 3$ ns as reported
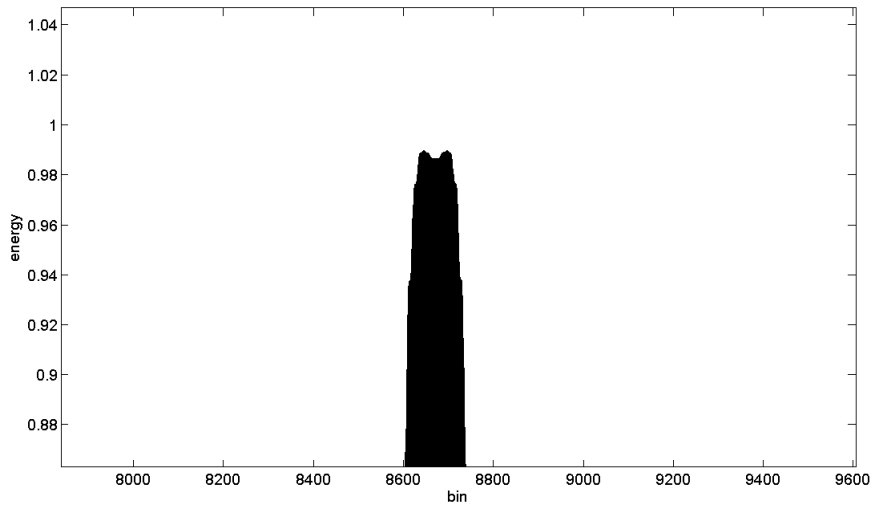
Figure 3.32: Energy profile around the maximum at 60 dB of SNR with $T_{int} = 2$ ns. $N_s = 1$.
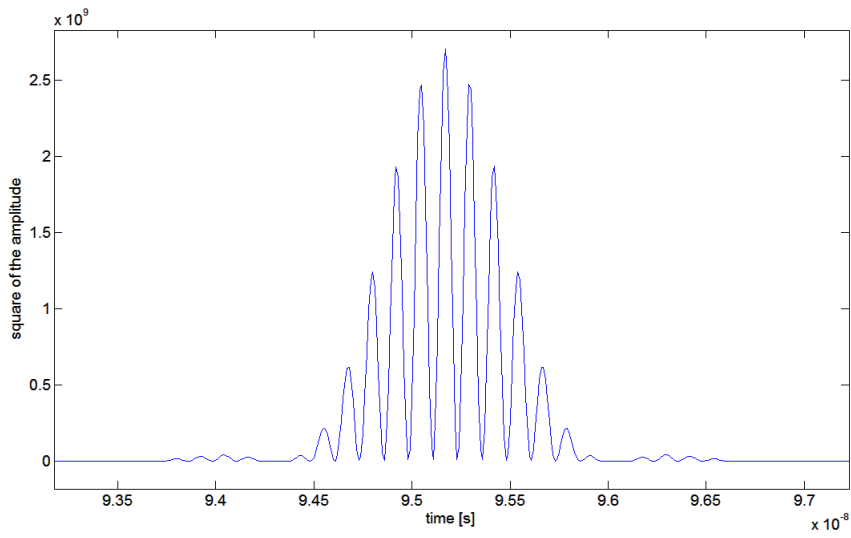
Figure 3.33: Square of the signal received for $T_p = 1$ ns. $N_s = 1$.

above.
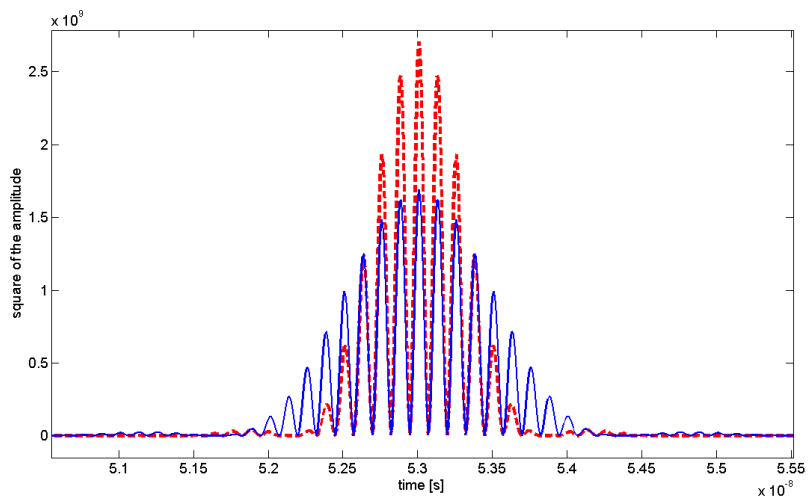
Figure 3.34: Square of the signal received for $T_p = 1$ ns (red dashed line) and $T_p = 1.6$ ns (blue solid line). $N_s = 1$.

A finally comparison useful to understand the real improvements in the performance that ML estimation introduces is the one reported in Fig. 3.35. As it can be seen from Fig. 3.35, a comparison between ML estimator for and *optimal thresholding* with the overlapping of the integration windows both with $T_{int} = 1$ shows how the ML estimator is always below and *optimal thresholding*. This is a good results that shows how the best algorithm which uses a threshold (*optimal thresholding*) is always worse than an ideal energy detector built from the theory for an ML estimator for unknown signals.
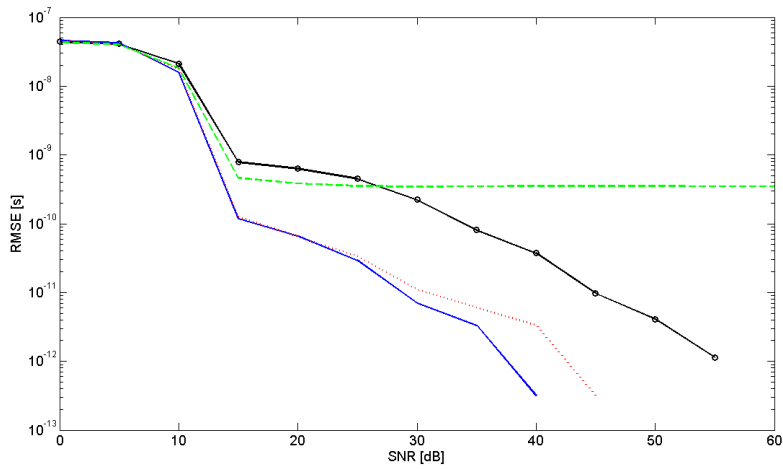
Figure 3.35: Performance comparison with ML estimator on AWGN channel for $T_p = 1.6$ ns. In blue solid line $T_{int} = 1$ ns, in red dotted line $T_{int} = 2$ ns, in green dashed line $T_{int} = 3$ ns and 'o' black line $T_{int} = 4$ ns. $N_s = 1$.
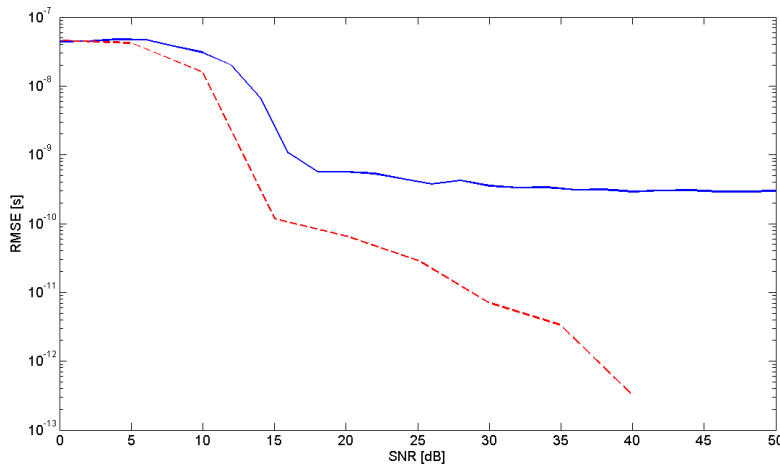
Figure 3.36: Performance comparison between *ML estimator* on AWGN channel for $T_p = 1$ ns and $T_{int} = 1$ ns (blue solid line) and *optimal thresholding* with the overlapping of the integration windows (red dotted line). $N_s = 1$.

Chapter 4

A real ToA estimator

In this chapter a practical ToA estimator used in SELECT project is shown, and its performance is investigated. Main issues and proposed solutions are analyzed and discussed.

4.1 Practical ToA estimator implementation

In the SELECT project some implementation constraints make necessary the adoption of a receiver scheme different from the one reported in Chap. 3. The available hardware layout developed by CEA-LETI (named *LORELEI*) is reported in Fig. 4.1. The signal received is at first amplified thanks to a Low Noise Amplifier (LNA); then two mixers centred at the central frequency of the transmitted signal (4 GHz) that down-convert the signal to base-band obtaining the in-phase I and quadrature Q components. The two vias are filtered with a low pass filter (LPF) with cut-off frequency of 500 MHz.
The second stage of LETI receiver (that will be described following) is composed of other 4 mixers used to shift the base-band components to an intermediate frequency to have 4 converted in phase and quadrature signals. An integration and dump stage follows each mixer, with integration time of 2 ns and "integrated bins" partially overlapped of 1 ns. Finally the analogue to digital conversion (ADC) is performed but for our purpose the ADC converter is neglected in the simulation.
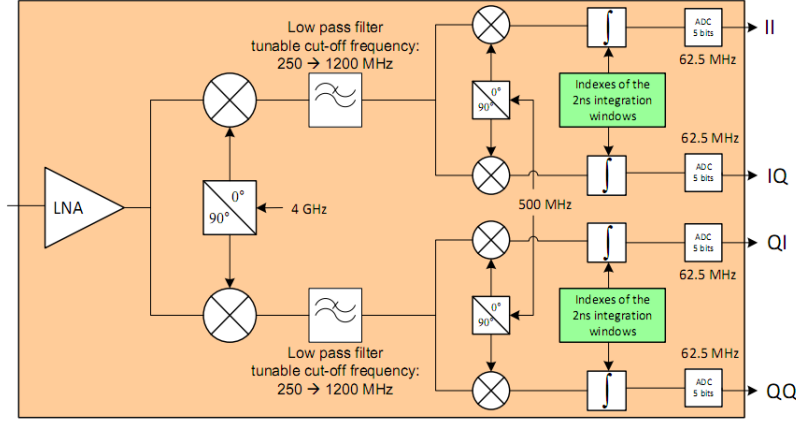
Figure 4.1: LORELEI LETI receiver layout [8].

4.2 Signal processing

Consider a received signal expressed as $r(t) = s(t) + n(t)$ (Fig. 4.2) composed only of the signal $s(t)$ and the AWGN noise $n(t)$ (interferences and multipath are not considered for simplicity). After the amplification, the signal is decomposed in in-phase and quadrature equivalents base-band ($\tilde{I}(t)$ and $\tilde{Q}(t)$), with expressions:

$$\tilde{I}(t) = r(t) \cdot cos(2\pi f_0 t + \varphi) \tag{4.1}$$

$$\tilde{Q}(t) = r(t) \cdot sin(2\pi f_0 t + \varphi) \tag{4.2}$$

where φ is a random phase identical for the 2 mixing stages (because generated by the same oscillator) and $f_0 = 4$ GHz.

The channel filtering is done by using a rectangular window, then the signals filtered are mixed again to an intermediate frequency and filtered by a low-pass filter (LPF with cut-off frequency of 500 MHz).
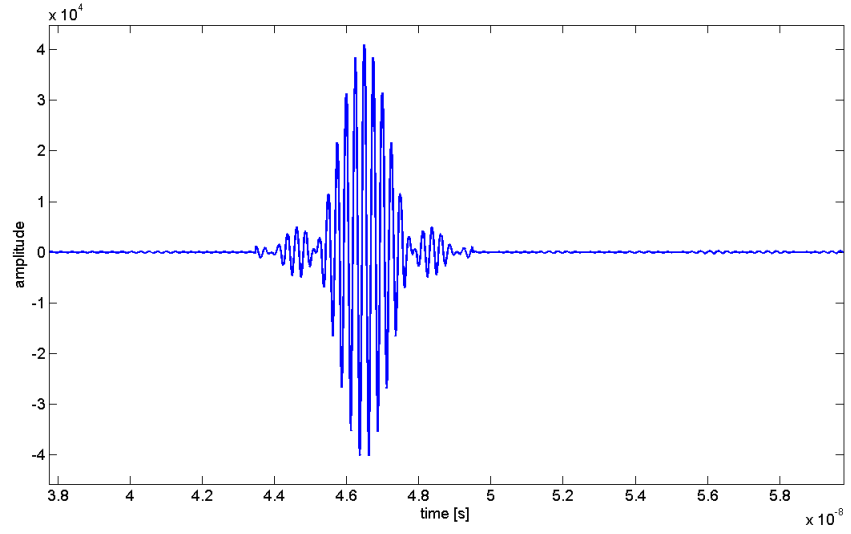
Figure 4.2: Example of $r(t)$ at 40 dB of SNR. Amplitude expressed in Volts.

The second mixing stage output are:

$$II(t) = I(t) \cdot cos(2\pi f_1 t + \varphi) \qquad (4.3)$$
$$IQ(t) = I(t) \cdot sin(2\pi f_1 t + \varphi) \qquad (4.4)$$
$$QI(t) = Q(t) \cdot cos(2\pi f_1 t + \varphi) \qquad (4.5)$$
$$QQ(t) = Q(t) \cdot sin(2\pi f_1 t + \varphi) \qquad (4.6)$$

whit $f_1 = 500$ MHz.
Now the integration stage is composed of four integrators, so at the
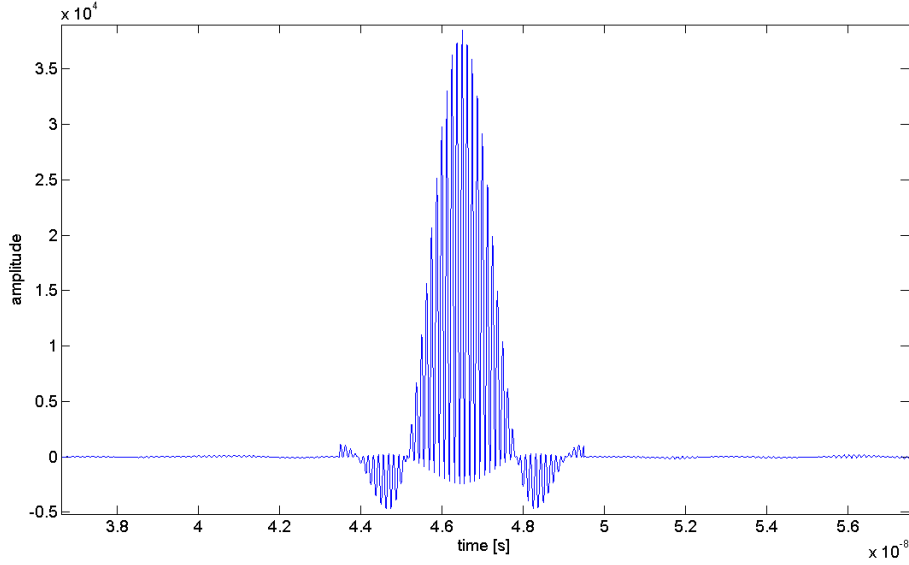
Figure 4.3: Example of $\tilde{I}(t)$ before the filtering. Amplitude expressed in Volts.

output of the receiver we have:

$$II_k = \int_{\xi_k}^{\xi_k+T_{int}} II(t)dt \qquad (4.7)$$

$$IQ_k = \int_{\xi_k}^{\xi_k+T_{int}} IQ(t)dt \qquad (4.8)$$

$$QI_k = \int_{\xi_k}^{\xi_k+T_{int}} QI(t)dt \qquad (4.9)$$

$$QQ_k = \int_{\xi_k}^{\xi_k+T_{int}} QQ(t)dt \qquad (4.10)$$

with

$$\xi_k = \begin{cases} (k-1)T_{int}, \ k = 1, 2, \cdots, 64 & case\ 1 \\ (k-1)\lfloor \frac{T_{int}}{2} \rfloor, \ k = 1, 2, \cdots, 128 & case\ 2 \end{cases} \qquad (4.11)$$

where (4.7), (4.8), (4.9) and (4.10) are the expressions of the k-th bin at the output of the integration stage an T_{int} is the integration window
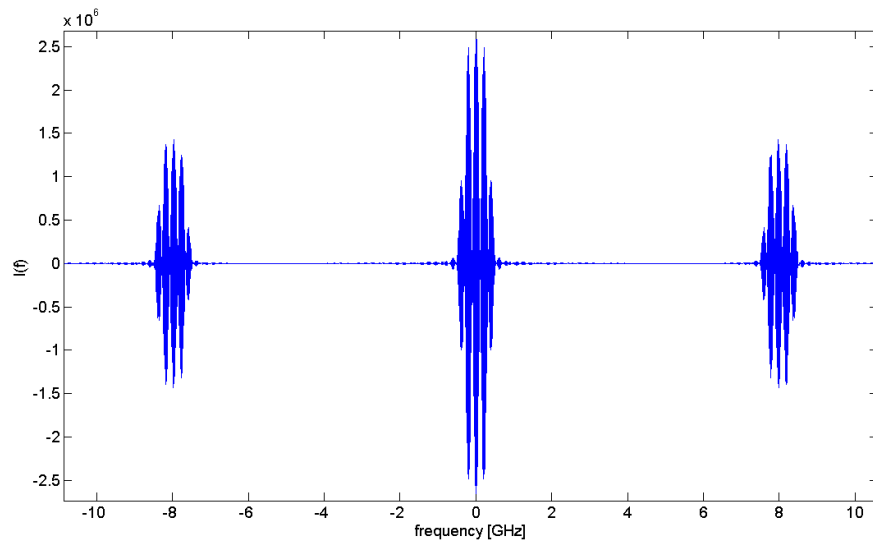
Figure 4.4: Spectrum of $\tilde{I}(t)$ before the filtering.
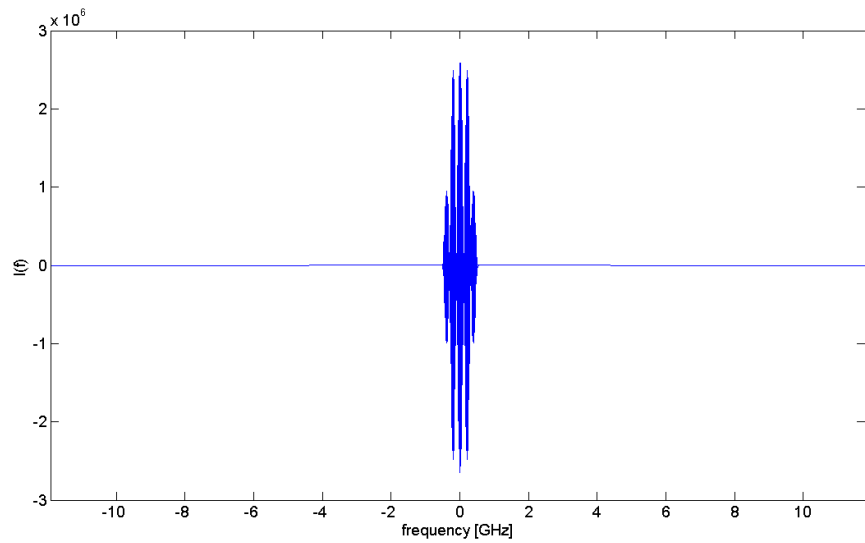
Figure 4.5: Spectrum of $I(t)$ after the filtering.
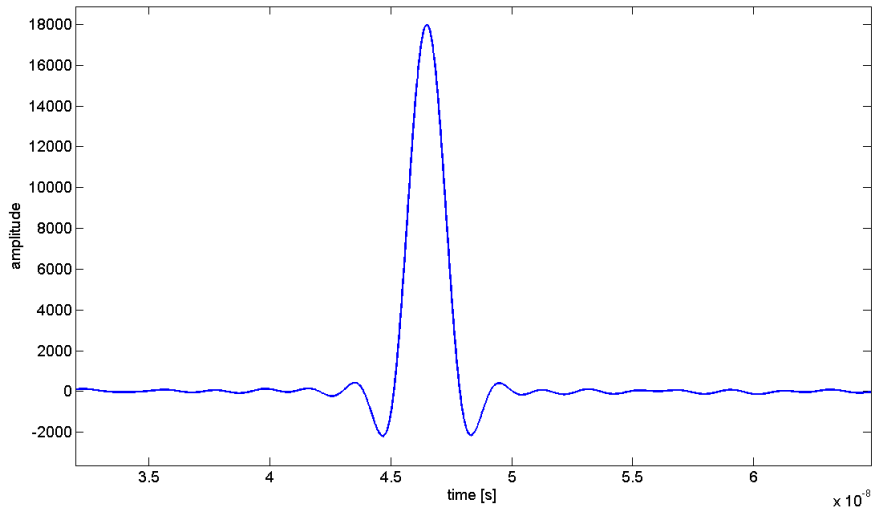
Figure 4.6: Example of $I(t)$ after the filtering. Amplitude expressed in Volts.
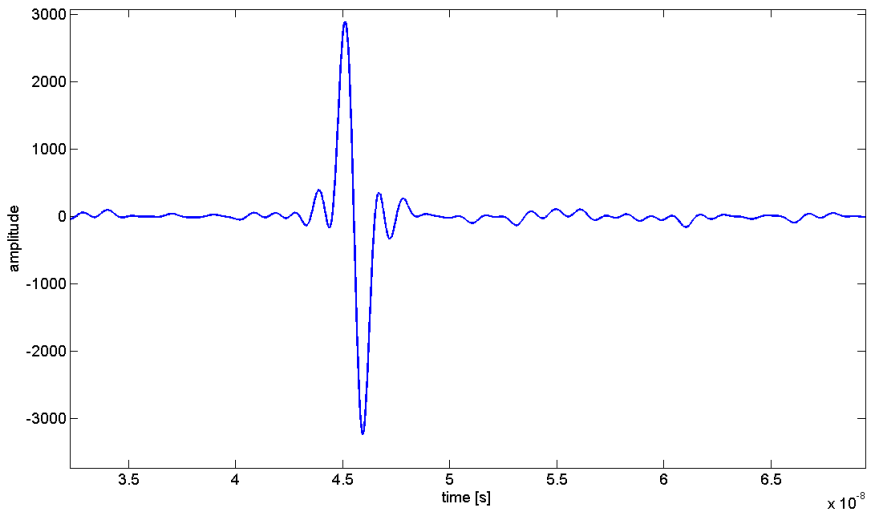
Figure 4.7: Example of $II(t)$ signal. Amplitude expressed in Volts.

of 2 ns. *Case 1* is used to build an energy profile without overlapping of the integration windows, instead *case 2* is used for the overlapping of the integration windows.

The method to build the "energy profile" (it is not a really energy profile, but in our receiver it is deputized to be it) is [8]:

$$Z_k = II_k^2 + IQ_k^2 + QI_k^2 + QQ_k^2 \qquad (4.12)$$

where Z_k is the k-th bin of energy; As the LETI hardware makes
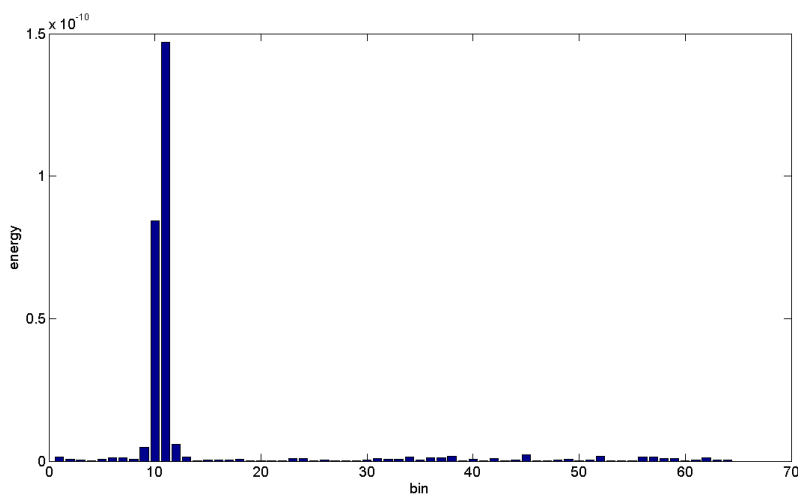
Figure 4.8: Example of energy profile calculated with (4.12) at 30 dB of SNR.

possible the partially overlapping of the integration windows, a smart thing to do is to exploit this possibility as has been done in Sec. 3.4.1. to increase the time resolution on ToA estimation. In this way, an energy profile with 1 ns of resolution (the same of Fig. 3.28) makes possible a more precise ToA estimation (*coarse estimation*). For further improving the ToA estimation, a *refined estimation* can be done by using the four output signals of the receiver. More in detail, once we have found the right bin (with index k) which contains the signal, we can refine the ToA estimation as reported below [8]:

$$\phi = \begin{cases} atan(IQ_k/II_k) & if\ (IQ_k^2 + II_k^2) \geq (QQ_k^2 + QI_k^2) \\ atan(QQ_k/QI_k) & if\ (IQ_k^2 + II_k^2) \leq (QQ_k^2 + QI_k^2) \end{cases}$$

with ϕ is the reconstructed phase of the signal. Then

$$TOA_{fine} = T_{int} \cdot \frac{\phi}{2\pi} \qquad (4.13)$$

where TOA_{fine} represents the value in ns which has to be used to correct the result of the coarse ToA estimation. Another method to implement the estimation refinement is the one which requires the implementation of a look-up table (LUT). In this way we make an approximation of the $atan(\cdot)$ function useful for a easier implementation on FPGA hardware. This is necessary because ToA estimation will be implemented in this kind of hardware, so a performance evaluation also with LUT is useful to understand pros and cons of this method.

4.3 Performance analysis and numerical results

In order to evaluate the performance of the described receiver, we built-in a simulator in Matlab that reproduces LETI hardware receiver reported in Fig. 4.1. In particular, we added a high-pass filter (HPF) with cut-off frequency of 20 MHz, for a greater adhesion with the reality (not indicated in Fig. 4.1). For our tests we have supposed to work in AWGN channel with a RRC signal in transmission. Parameters of transmitted signal (Fig. 4.2) are:

- $T_p = 1.6$ ns that ensures a bandwidth of $B = \frac{1+\beta}{T_p} = 1$ GHz (where $\beta = 0.6$ is the roll-off factor);

- unitary-energy pulse;

- 128 ns of frame duration;

- $N_s = 1$ symbol transmitted.

To emulate different propagation delays, a random delay τ is generated and applied to the signal time of arrival. In particular τ is uniformly distributed between 4 and 74 ns to reproduce a real propagation of the signal in scenario where the tags are uniformly distributed from 0.6 to 11.1 m from the reader ($\tau = RTT$ so $d = \frac{RTT \cdot c}{2}$ where $c = 3 \cdot 10^8$ m/s).

In addition, for a more precise ToA estimation, overlapped integration windows have been used. No threshold has been used for ToA estimation, but a max search algorithm has been implemented. In fact the ToA is estimated choosing the bin that contains the maximum energy.

Fig. 4.9 shows the performance of LETI receiver with the 3 algo-
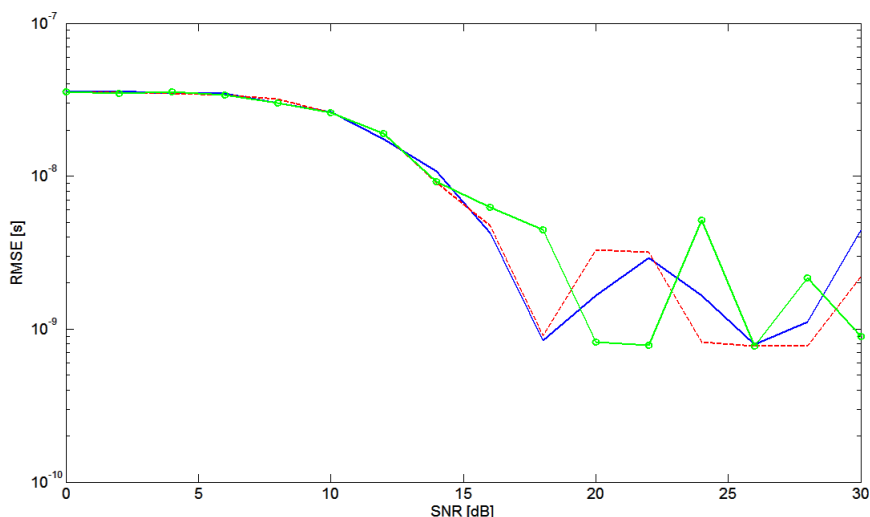
Figure 4.9: Performance of LETI receiver for coarse ToA estimation (blue solid line), refined ToA estimation with $atan(\cdot)$ function (red dashed line), refined ToA estimation with LUT ('o' green line). All curves with $\varphi = 0$ have been done.

rithms proposed for coarse and refined ToA estimation. In this figure phase φ is not considered for mixing stage. The floor of $T_{int}/\sqrt{12}$ is not reached, moreover with refined estimation we do not observe any improvements for ToA estimation. The oscillations for high SNRs are due to the fact that in some cases the energy profile is not composed of a peak in the center of the signal (ToA), but it has a profile as reported in Fig. 4.11.

The algorithm makes the choice for one of the two peaks around the bin that contains the true ToA of the signal, leading to an incorrect estimation and consequently to a RMSE value far from the ideal floor. To mitigate this phenomenon, a modification on the energy
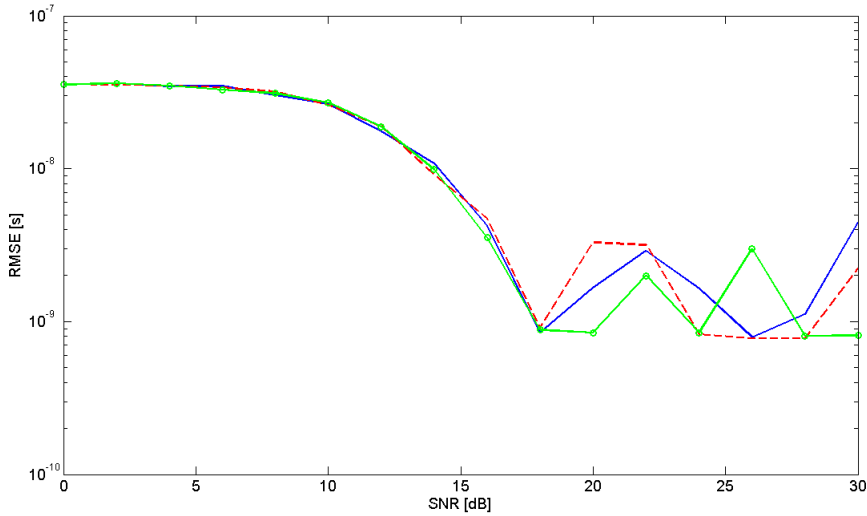
Figure 4.10: Performance of LETI receiver for coarse ToA estimation (blue solid line), refined ToA estimation with $atan(\cdot)$ function and $\varphi = 0$ (red dashed line) and refined ToA estimation with $atan(\cdot)$ function with φ as uniform r.v. on 2π.

profile construction is proposed and analyzed in the following. Fig. 4.10 shows as the introduction of a random phase does not modify the performance of our estimator because we make an error far from the theoretical floor.

4.3.1   Improvements on ToA estimation

Addition of LPF   The first improvement useful for obtaining better performance (reach the theoretical floor) on ToA estimation with LETI receiver is the **introduction of a low-pass filter** (with 500 MHz cut-off frequency) after the second mixing stage (downstream of the HPF). With this filter, that however cuts a useful part of the signal spectrum, we are able to improve the performance as shown in Fig. 4.12. The reason for this behaviour is not totally understood, so this may be a case study to clarify what happens to the signal to have a
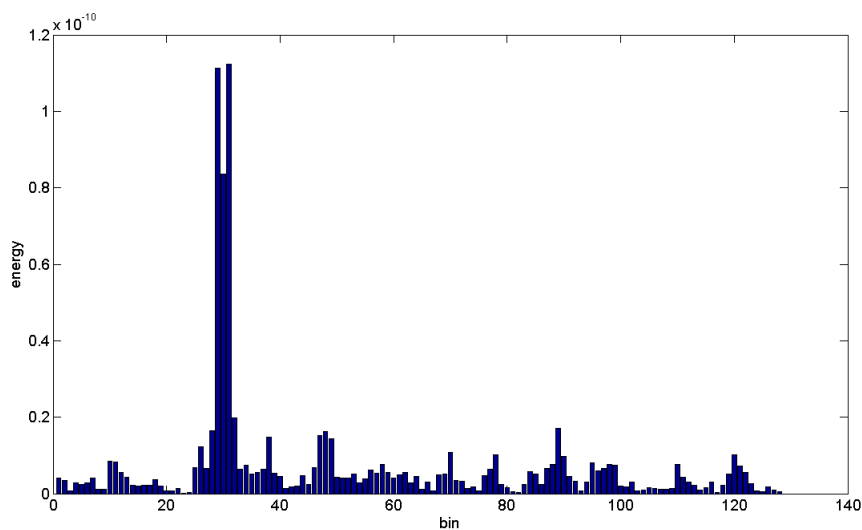
Figure 4.11: Energy profile with LETI receiver using the integration windows overlapped. SNR=30 dB.

performance improving. Starting our analysis from Fig. 4.12 we note that with the second LPF we can reach the floor of $T_{int}/\sqrt{12} \simeq 0.29$ ns for coarse ToA estimation (remember that with integration windows overlapped we have a 'virtual' T_{int} of 1 ns). Refined ToA estimation moves this floor down of about 1 ns, making possible ranging with about 3.6 cm of precision. Refined estimation with LUT still moves down the floor, but not as good as the $atan(\cdot)$ implementation as it is an approximation, with ranging precision of about 6 cm. By analyzing Fig. 4.13, we note that the presence of a random phase inside the mixing steps introduces a worsening on the performance related to the refined ToA estimation. Unfortunately in real cases we have to work with this random phase, so refined ToA estimation should not to be considered to do not aggravate ToA estimation.
This improvement in ToA estimation however can be used only if the hardware can be modified by inserting the LPF above mentioned.

Signal bandwidth improvements For ToA coarse estimation, there is also another method to reach the theoretical performance of
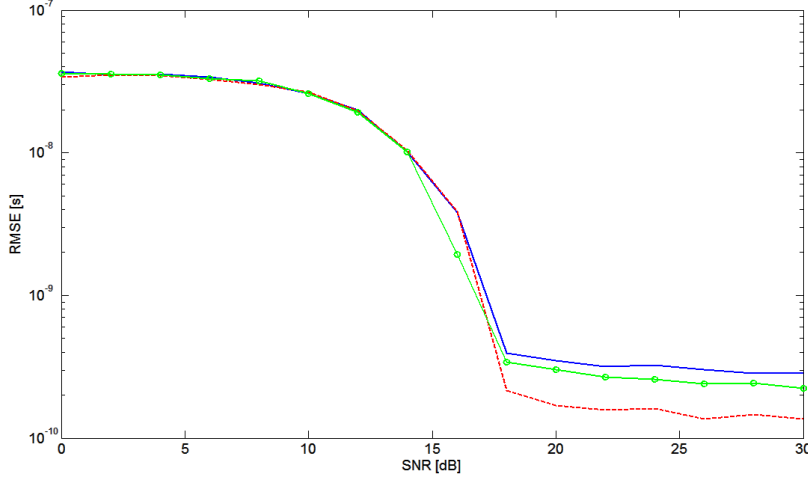
Figure 4.12: Performance of LETI receiver with LPF after HPF for coarse ToA estimation (blue solid line), refined ToA estimation with $atan(\cdot)$ function (red dashed line), refined ToA estimation with LUT ('o' green line). All curves have been obtained imposing $\varphi = 0$.

0.29 ns, **playing with the signal bandwidth**. In fact enlarging the bandwidth of the transmitted pulse, we obtain a signal with shorter time duration, so great part of the energy of the signal is inside only one integration window making possible a more precise ToA estimation. This behaviour is shown in Fig. 4.14 and the theoretical floor is reached by a value of bandwidth of 2-2.25 GHz.

Before using this method is necessary to check that the bandwidth of the transmitted signal satisfies the requirements imposed by FCC or other administrative bodies on spectrum usage.

Energy profile modification   The last approach proposed to improve the performance of the LETI receiver is a **variant on the construction of the energy profile**. Starting with the energy profile given as (4.12), we can modify it with the following algorithm:

$$Z_{k_{new}} = Z_{k-1} + Z_k + Z_{k+1} \tag{4.14}$$
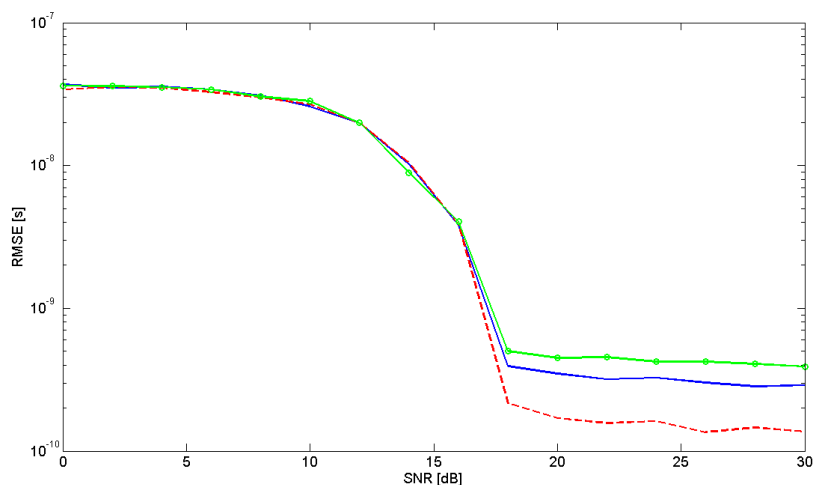
Figure 4.13: Performance of LETI receiver with LPF after HPF for coarse ToA estimation (blue solid line), refined ToA estimation with $atan(\cdot)$ function and $\varphi = 0$ (red dashed line) and refined ToA estimation with $atan(\cdot)$ function with φ as uniform r.v. on 2π.

where $Z_{k_{new}}$ denotes the k-th energy bin of the *new energy profile*.

With this approach we obtain an energy profile that avoids the problem of Fig. 4.11, and ensures theoretical performance for coarse ToA estimation. Also refined ToA estimation takes advantage of this method. In fact we use this new energy profile to detect the correct bin that includes the max of the signal, and after that we apply the algorithm for refining ToA estimation. The new energy profile is reported in Fig. 4.15.

From Fig. 4.16 we observe a very good performance with $atan(\cdot)$ function in the case where φ is not considered. In this case, the floor reached is of 60 ps, which equals to 1.8 cm in ranging precision. Look-up table also improves the precision, but only of 0.05 ns, so in this case, the approximation introduced on $atan(\cdot)$ function is not negligible.

Unluckily φ has to be considered for real scenario, so we refer to Fig. 4.17, and in particular to the green 'o' line. As it can be noticed, the performance for refined estimation are worse than the coarse estima-
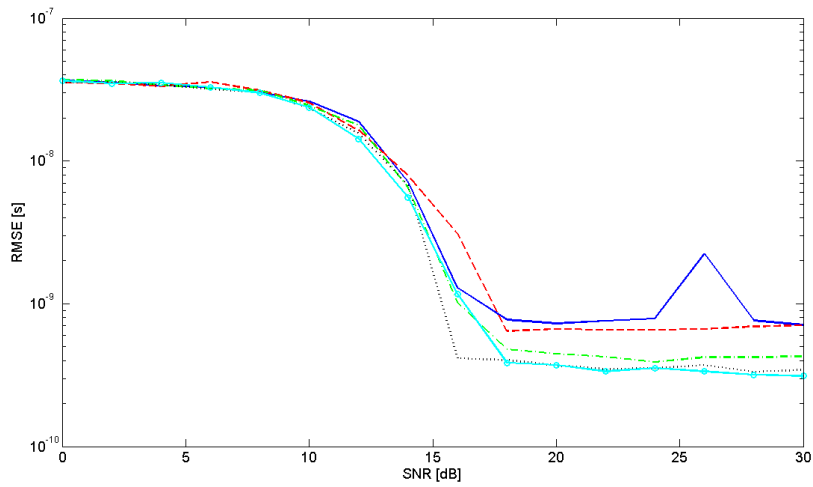
Figure 4.14: Performance of the LETI receiver with different bandwidth for the transmitted signal with coarse ToA estimation. In blue solid line B=1.25 GHz, in red dashed line B=1.5 GHz, in green dashed dotted line B=1.75 GHz, in black dotted line B=2 GHz and finally in chain 'o' line B=2.25 GHz.
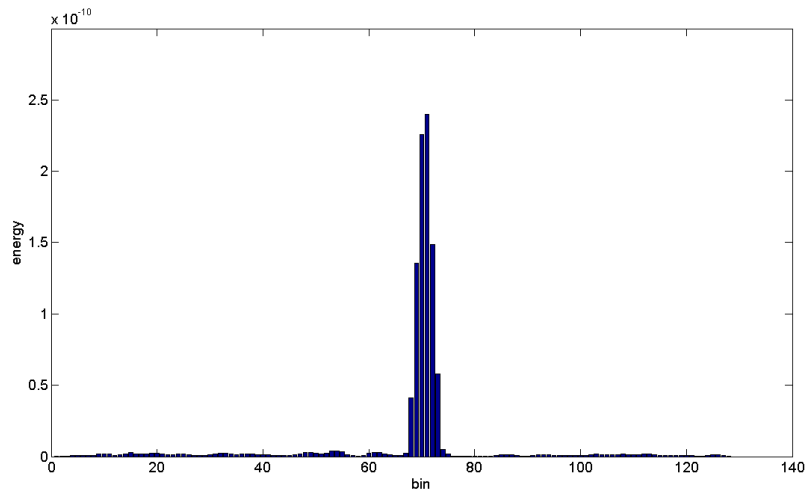
Figure 4.15: Example of energy profile built with (4.14).
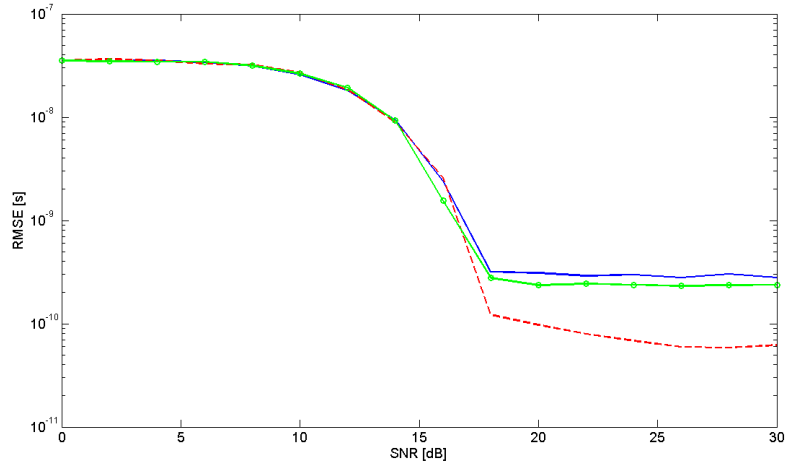
Figure 4.16: Performance of LETI receiver with energy profile modified for coarse ToA estimation (blue solid line), refined ToA estimation with $atan(\cdot)$ function (red dashed line) and refined ToA estimation with LUT ('o' green line). $\varphi = 0$ for all curves.

tion when we consider the random phase in mixing stage.

This approach ensures good performance with AWGN channel and only a single path. Will be interesting to investigates the performance also for a multipath channel or with some interferences to reproduce the behaviour of a real propagation channel.
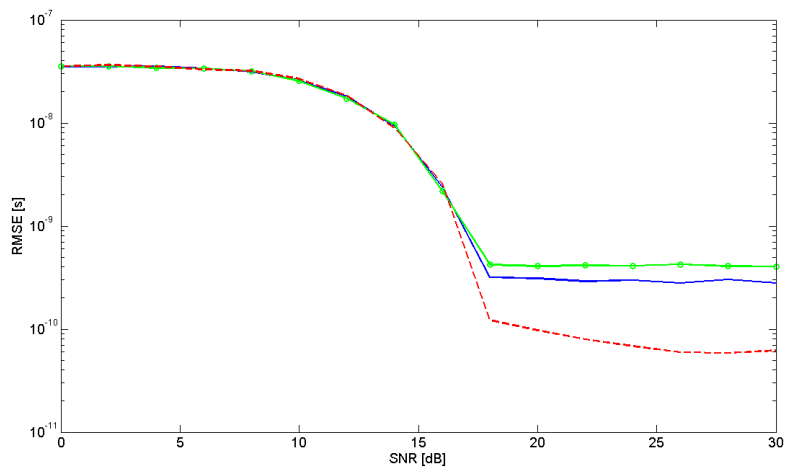
Figure 4.17: Performance of LETI receiver with energy profile modified. In blue solid line coarse ToA estimation; in red dashed line refined ToA estimation with $atan(\cdot)$ function ($\varphi = 0$) and in 'o' green line refined ToA estimation with $atan(\cdot)$ function ($\varphi \sim \mathcal{U}(0, 2\pi)$).

Conclusions

RTLSs are one of the fields that is becoming important nowadays. Make the correct ranging estimation is the base for this systems, and one way to implement this ranging technique is the ToA estimation. In this work a focus on ToA estimation techniques has been done. At first, different theoretical techniques have been investigated, and after that a real ToA implementation has been studied.

From the results reported in Sec. 3.3 we understood how sub-optimal algorithms have not performances as good as optimal thresholding algorithm. This suggests that every algorithm that may be implemented never gives optimal performance because optimal performance is given only by optimal thresholding algorithm that bases its functionality on a-priori information, and in real applications this information is usually unknown. Another method for ToA estimation is the ML estimation with which we have been able to understand what is the theoretical limits of the performance given by algorithm not based on thresholding.

Moving our attention on the analysis of a real ToA estimator, we have studied its performance in a simplified case (AWGN channel model) to understand how it works, and if theoretical limits can be reached. By a first analysis some problems to ensure good performance have emerged; in fact looking at the results of Sec. 4.3 we note that ideal performance are far from the one reached. To improve the performance some empirical methods have been tested, and several of them make possible the achievement of theoretical performance. Unluckily these methods work well under a simplified hypothesis, rarely verified in real applications; however the possibility of reaching theoretical bounds in some cases shows how a more detailed study on the real estimator tested may lead to the achievement of the target.

May be interesting to investigate the performance of the real ToA estimator in a different channel model (for example with multipath and interference) and by the application of more complicated estimation techniques to detect the first path for ToA estimation. These and many other tests can be done to fit the real scenario applications for the estimator tested.

Acknowledgements

Starting by the consideration that if I were to list all the people to which I am grateful probably I have to write another chapter, I want to start my acknowledgements from my professor Davide Dardari and his assistants Nicoló Decarli and Francesco Guidi. They had give to me a magnificent opportunity to improve my knowledge in a new research field as RTLSs. I also would to thank all the research group in telecommunication of Via Venezia 52 (university of Bologna at Cesena) for helpful suggestions during my thesis period.

A particular thanks goes to my family: my mother Liviana and my father Fabio for economical support and my brother Giovanni for all the sleepless nights passed with the computer turned on for the simulations. But my family is also composed by my girlfriend Francesca. I would to thanks especially she for putting up with me and motivated in difficult times and stress. I have not got a good character when I am stressed, and she has been able to bring out the best of me.

I also would to thanks all my relatives, who are with me and who look at me by the sky, my friends with which I have spent free time to relax and enjoy myself, and my colleagues for the technical support to write this thesis. Thanks to all that have believed in me.

Bibliography

[1] www.selectwireless.eu

[2] D. Dardari, E. Falletti, M. Luise: *Satellite and Terrestrial Radio Positioning Techniques*, A signal processing perspective, Academic Press.

[3] D. Dardari, F. Guidi, Christophe Roblin and Alain Sibille: *Ultra-Wide bandwidth backscatter modulation: processing schemes and performance*, EURASIP Journal on Wireless Communication and Networking, vol. 2011, no. 1, 2011.

[4] D. Dardari, A Conti, U. Ferner, A. Giorgetti, M. Z. Win: *Ranging With Ultrawide Bandwidth Signals in Multipath Environments*, PROCEEDINGS OF THE IEEE, 2009, 97, pp. 100 - 122.

[5] A Conti, M. Guerra, D. Dardari, N. Decarli, M. Z. Win: *Network Experimentation for Cooperative Localization*, IEEE Journal on Selected Area in Communications, Special Issue on Cooperative Networking - Challenges and Applications, vol. 30, no. 2, 2012.

[6] I. Guvenc, Z. Sahinoglu, A. Molisch, P. Orlik: *Non-Coherent TOA Estimation in IR-UWB Systems with Different Signal Waveforms*, MITSUBISHI ELECTRIC RESEARCH LABORATORIES, IEEE International Conference on Broadband Networks, pp. 245-251, October 2005.

[7] M. Chiani: *Notes on detection and estimation*, course of "Sistemi di telecomunicazioni LM" University of Bologna at Cesena.

[8] D. Dardari: *Signal processing techniques: Interim report*, Deliverable D2.2.1, Work Package 2, Dissemination level PU, lug-2011, SELECT project.

[9] C. Falsi, D. Dardari, L. Mucchi, and M. Z. Win, "Time of arrival estimation for UWB localizers in realistic environments," EURASIP J. Appl. Signal Processing (Special Issue on Wireless Location Technologies and Applications), vol. 2006, article ID 32082, 13 pages.